CBX 97-106
December 1997

Search for CP violation in tau decay

C Jessop

SLAC

A difference in the partial decay amplitudes of the τ^- and τ^+ leptons is evidence of CP violation. This can arise in extensions to the standard model in which the interference of the additional CP violating contributions with the standard model amplitudes can result in observable asymmetries. In this note we assess the possible ways in which CP violation can be observed in the tau lepton system at CLEO. We define an experimentally observable asymmettry (A^+_{cp},A^-_{cp}) which could be as large as (-3.3 %,3.3 %). We report on the first ever search for CP violation in lepton (tau) decay using this asymmetry definition in the most promising $K\pi\nu$ decay channel. We measure an asymmetry of (A^-_{cp}= 0.9 ± 3.7 %,A^+_{cp} -1.0 ± 3.9 %). No statistically significant evidence is found for CP violation in tau decay.

1 Introduction

The origin of CP violation is not well understood. In the language of field theory CP violation arises from a non-zero phase in the coupling constant which changes sign under the combined operations of CP. In the standard model this phase arises from a complex degree of freedom in the quark mixing matrix (CKM) that appears after symmetry breaking. In this model CP violation is confined to the quark sector and so we would expect no CP violation in lepton couplings. However there is no fundamental reason why CP violation should be confined to the quark sector. If for example the three generations of neutrinos have non-zero and non-degenerate mass then a mixing matrix arises in the lepton sector in analogy with the CKM case and the complex degree of freedom can give rise to CP violating lepton couplings [1].

The effects are too small to be currently measurable but experimentally significant lepton CP violation can arise in many extensions to the standard model [10]. For example Lee and Weinberg [11] [12] have pointed out that in theories with multi-Higgs doublets CP violation can occur naturally via the complex couplings of both neutral and scalar Higgs. This example is described in detail in appendix A.

The standard model explanation of CP violation is not experimentally confirmed. As CP violation is the only way to define matter as opposed to anti-matter it seems likely that CP violating interactions play a fundamental role in the origin of the matter-antimatter asymmetry in the universe [2]. The most reasonable theory of the origin of this asymmetry is the theory of baryogenesis [3] described in appendix B. If the standard model of CP violation is used in this model it fails to account for the observed asymmetry by 10-14 orders of magnitude [4]. This could suggest that there are additional sources of CP violation beyond the standard model. A search for CP violation in areas which the standard model prohibits may help solve this problem. We first describe some general considerations for CP violation before describing the experimental ways in which it might be observed.

2 General Considerations for CP violation

CP violation is the observable difference between a process ($a \to b$) and its CP conjugate ($\overline{a} \to \overline{b}$). CP violation enters into the Lagrangian for a physical process as a phase which changes sign under the operation of CP (i.e a CP odd complex coupling)

$$CP : e^{i\theta} \to e^{-i\theta}$$

Since the absolute value of a phase is not physically meaningful CP violation can only be observed when interfered with another phase δ that does not change under the operation of CP

$$CP : e^{i\delta} \to e^{i\delta}$$

This can be understood by considering a process that has two different amplitudes A_1 and A_2. They have a relative CP odd phase θ and a relative CP even phase δ. The probability density is given by the square of the matrix element

$$P^+ = \mid M \mid^2 = (A_1 + A_2 e^{i(\delta-\theta)})(A_1 + A_2 e^{-i(\delta-\theta)}) = \mid A_1 \mid^2 + \mid A_2 \mid^2 + 2A_1 A_2 \cos(\delta - \theta)$$

The CP conjugate process is then described by

$$P^- = \mid M \mid^2 = (A_1 + A_2 e^{i(\delta+\theta)})(A_1 + A_2 e^{-i(\delta+\theta)}) = \mid A_1 \mid^2 + \mid A_2 \mid^2 + 2A_1 A_2 \cos(\delta + \theta)$$

There is no difference between the probability densities, and thus all physical observables, unless all the following conditions are satisfied.

$$\begin{aligned} A_1 &\neq 0 \\ A_2 &\neq 0 \\ \delta &\neq 0 \\ \theta &\neq 0 \end{aligned}$$

This interference can occur in several different ways which are briefly described below after a comment on CPT violation

2.1 CPT violation

CPT symmetry is a fundamental assumption of field theory [5] and is consistent with all experimental observations to date. It requires that the Lagrangian for the decay be hermitian. For the coupling above

$$CPT : Ae^{i\theta} \rightarrow A_{CPT} e^{-i\theta_{CPT}}$$

CPT symmetry requires:

$$\begin{aligned} A &= A_{CPT} \\ \theta &= -\theta_{CPT} \end{aligned}$$

Hence if a, b and $\overline{a}\overline{b}$ are also CPT conjugates and CPT symmetry holds then in order to observe CP violation the phase $\delta \neq 0$. i.e. if we observe a difference in the processes $(a \rightarrow b)$ and its CP conjugate $(\overline{a} \rightarrow \overline{b})$ and there is no phase δ involved in the process then we are actually observing CPT violation since they are also CPT conjugates. We also note that since CPT implies the equivalence of particle and anti-particle lifetimes the total decay rates of τ^- and τ^+ must be equivalent and CP violation can only be observed in exclusive modes.

3 Observing CP violation

There are three ways to observe CP violation, in mixing, in decay and in dipole moments. We describe each here for the purpose of assessing how to observe CP violation in tau leptons.

3.1 CP violation in mixing

The neutral meson systems $(M_0, \overline{M_0}), [M = K, D, B]$ are produced by the strong interaction but can only decay by the weak interaction. Since M_0 and $\overline{M_0}$ are particle and anti-particle distinguished only by their flavor and the weak interaction is flavor violating mixing is possible. The mixing process for $\mid M >= \mid (M_0, \overline{M_0} >$ is described by the Hamiltonian

$$i\frac{d \mid M >}{dt} = (m + i\Gamma) \mid M >$$

where m and Γ are the mass and decay matrices. The eigenstates are not particle and anti-particle and so can have a mass difference which is given by the real part of the difference of the eigenvalues Δm. The oscillation frequency is given by the mass difference. Thus a mixed and unmixed particle differ by a CP even phase $e^{i\Delta mt}$ at a time t. This phase can be used to interfere with the CP odd weak phase. For example in the B meson system if we consider a final state which is a CP eigenstate accessible to both B_0 and $\overline{B_0}$ then the two amplitudes which interfere are the decay of the mixed and unmixed particle which differ by a CP even phase Δm and a CP odd phase (which is presumed to come from the KM matrix in the standard model explanation of CP violation) [6].

3.2 Direct CP violation

An amplitude can have two parts a real or dispersive part and an absorptive or imaginary part. The dispersive component is from transitions with virtual (off mass shell) intermediate states and the absorptive from real (on mass shell) intermediate states. For example in the case of mixing the dispersive part is the mass matrix and the absorptive is the decay matrix. The absorptive part of an amplitude gives a CP even phase which can be used to interfere with a CP odd phase and thus give CP violating effects without

the need for mixing. To illustrate this we consider another example from the standard model explanation of CP violation - the interference of the tree and penguin diagrams in the decay of the B meson [7]. Figure 1 shows the two interfering amplitudes. The penguin diagram has an absorptive component which occurs when the u and c intermediate quark states are on shell (the t is too heavy). The magnitude of the absorptive part is different for u and c . The CKM phases are different for the tree and penguin and between the u and c penguin so that we can get CP violation not only from tree-penguin interference but also penguin-penguin interference.

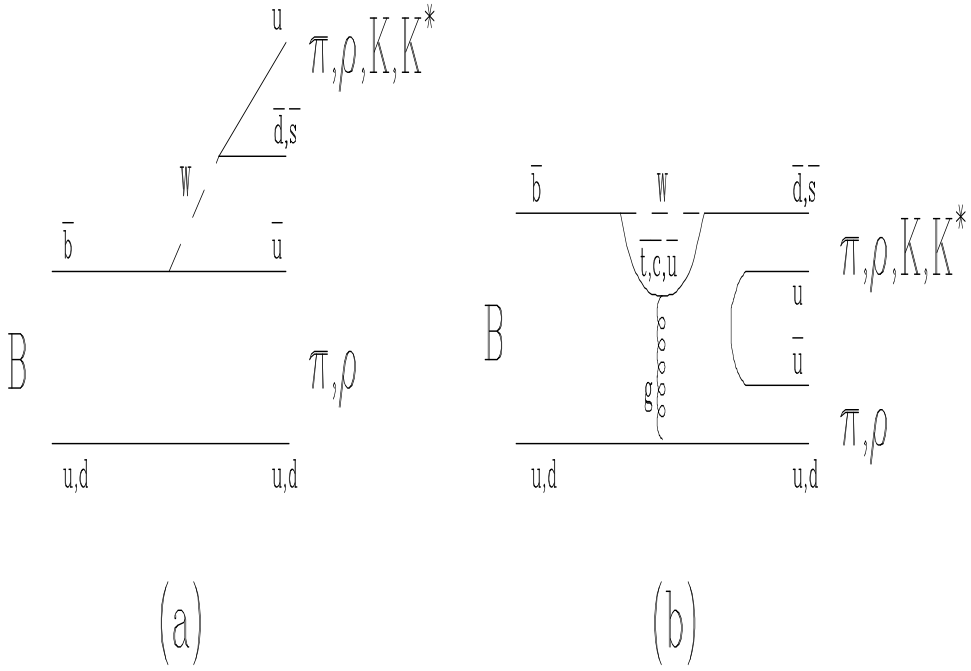

Figure 1: The two amplitudes for $B \to K\pi$. The tree level diagram and the penguin can interfere to give direct CP violation

3.3 Dipole Moments

Table 1 shows the T and P transformation properties of classical quantities. A dipole moment arises classically when the center of the charge

Quantity	T	P	
r(position)	r	-r	polar vector
p(momentum)	-p	-p	polar vector
S(spin)	-S	S	axial vector(S=r×p)
E(electric Field)	E	-E	(E=-dV/dr)
$S \cdot E$	-S·E	-S·E	Electric Field
$S \cdot p$	$S \cdot p$	$-S \cdot p$	Longtitudal polarization
$S \cdot (p_1 \times p_2)$	$-S \cdot (p_1 \times p_2)$	$S \cdot (p_1 \times p_2)$	transverse polarization

Table 1: Transformation under T and P of classical quantities

distribution is not the center of the mass distribution and is T violating. Assuming that CPT is conserved this then implies that a dipole moment is CP violating. An elementary particle with an electric dipole moment is thus both T and CP violating.

Figure 2: The dipole moment amplitude can interfere with the tree level amplitude to give CP violation

In quantum field theory a T transformation is associated with $i \to -i$ and therefore a T violating interaction appears in the Lagrangian as a purely imaginary term which corresponds to loop diagrams as in figure 2.

$$L_{cp} = -i\overline{\psi}(p_2)\sigma_{\mu\nu}\gamma_5\psi(d_{em}(q^2 = 0)F^{\mu\nu} + d_w(q^2 = M_Z)Z^{\mu\nu})$$

$F^{\mu\nu}$ and $Z^{\mu\nu}$ are the field tensors for the photon and Z boson, d_{em} and d_w are the electric and weak dipoles and $q = p_2 - p_1$. These interactions

can only appear at the loop level since they are non-renormalizable at tree level [8]. Since the dipole coupling is always imaginary we can observe the CP violating effects by interference with the tree amplitude as in figure 2 without the need for a strong phase. Note that his type of CP violation does not occur until the three loop level in the standard model and so is extremely suppressed. However in extensions to the standard model in which a neutral boson appears in the loop much larger effects can occur. An example of this type of CP violation would occur in neutron electric dipole moments [8].

3.4 Direct CP violation from additional charged bosons

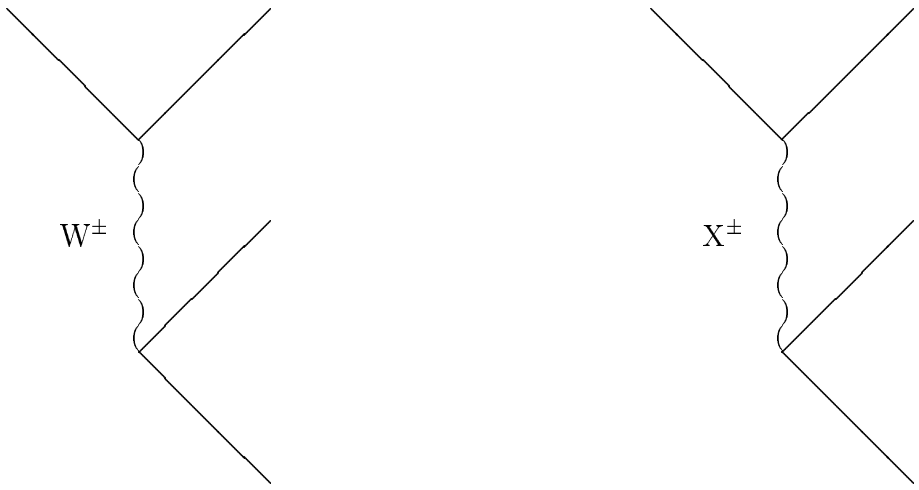

Figure 3: An additional charged boson can interfere with the standard model W to give CP violation if there are complex coupling constants

The introduction of an additional neutral boson with CP violating couplings can lead to CP violation through dipole moments as above. Similarly the introduction of charged bosons with CP violating couplings can lead to CP violation effects. Consider the decay of a charged particle as in figure 3. The decay can proceed through the standard model W boson or through the new X boson. We require the two diagrams to have a relative CP odd weak phase and CP even strong phase. The strong phase can occur in final

state interactions when the decay products are quarks. The magnitude of this strong phase depends on the angular momentum and isospin of the final state and so if the two diagrams have either different isospin or angular momentum the CP violation is possible. An example of this type of CP violation could occur in hyperon decays [9]. The standard model decay proceeds by the p or s wave decay since it is a vector particle and if the charged X is a scalar then it proceeds via the S wave. Since the strong phases of the two amplitudes can be different CP violation can be observed if there is a relative CP odd weak phase between the two amplitudes.

4 Observing CP Violation in Taus

The CP conjugate of τ^+ is τ^-. Since they are also particle and anti-particle they are in addition CPT conjugates. Since the tau is charged there can be no mixing. Only direct CP violation is possible. There are two possibilities. CP violation due to an electric dipole of the tau which requires an additional neutral boson beyond the standard model or CP violation in the decay which requires an additional charged boson. It is possible to search for both possibilities at an electron-positron machine.

4.1 CP violation from a tau electric dipole moment

Consider the process

$$e^+(p_+) + e^-(p_-) \rightarrow \tau^+ + \tau^- \rightarrow A^+(p_A) + B^-(p_B) + \nu_\tau \overline{\nu_\tau}$$

where A^+ and B^- are the charged hadronic or leptonic final states. We can define observables sensitive to the dipole moments.

$$\begin{aligned} < O^- > &= \frac{\sqrt{s}}{e} c_{AB} Re(d_w) \\ < O^+ > &= \frac{\sqrt{s}}{e} c_{AB} Im(d_w) \end{aligned}$$

$< O^- >$ is CP odd and CPT even while O^+ is CP odd and CPT odd. A CPT odd variable must be proportional to the absorptive (imaginary) part

of the dipole moment, while a CPT even variable must be proportional to the real part. This is because the CPT transformation is equivalent to hermitian conjugation as explained above. c_{AB} are the experimental sensitivities which are different for each mode. CP violation then implies a non-zero expectation value of these observables. It is possible to define many observables of this form [15] but the optimal (in terms of signal to noise) observables have been defined and used in recent analysis [16].

$$\begin{aligned} < O^- > &\propto \frac{\sigma_-}{\sigma_{SM}} \\ < O^+ > &\propto \frac{\sigma_+}{\sigma_{SM}} \end{aligned}$$

where

$$\begin{aligned} \sigma_- &= (k^+.q_e)(k^+ \times (S^+ - S^-)).q_e \\ \sigma_+ &= 1 + (k^+.q_e)^2 + S^+S^-(1 - (k^+.q^e)^2 \\ &\quad -2(q_e.S^+)(q_e.S^-) + 2(k^+.q_e \\ &\quad [(k^+.S^+)(q_e.S^-) + (k^+.S^-)(q_e.S^+)] \\ \sigma_{SM} &= (K^+.q_e[(k^+.S^+)(q_e.S^-) - (k^+.S^+)(q_e.S^+) \end{aligned}$$

k^+ is the flight direction of the positive tau and $S^\pm$ are the spin directions of the positive and negative tau in the tau's rest frame. Neither the tau flight direction nor the spin direction can be measured directly. If there is only one neutrino in the tau decay (i.e non-leptonic decays) then the tau flight direction lies on a cone about the hadron vector (i.e the vector sum of the measured hadronic decay particles). The half-angle of the cone can be determined if the energy of the tau can be assumed to be the beam energy (i.e no initial state radiation). If both taus are non-leptonic then the intersection of the two cones determines the direction of the tau to a two fold ambiguity and further the ambiguity can be resolved with a precision vertex detector [17]. The spin direction can be inferred by recognizing that the width of a tau decay contains terms $S.k$ where k is the flight direction and S the spin [19] and hence that the measurement of the energy and momentum of the decay particles can be combined with knowledge of the flight direction to infer the spin direction [20]. No evidence of CP violation in tau production

has been observed using the full LEP data sets and the current 95 % limits on tau dipole moments are [21]

$$\begin{aligned} \mid Re(d_w) \mid &< 3.6 \times 10^{-18} ecm \\ \mid Im(d_w) \mid &< 1.1 \times 10^{-17} ecm \\ Re(d_w) &< 1.1 \times 10^{-17} ecm \end{aligned}$$

A similar analysis could be performed at the lower energy of CLEO ($\sqrt{s} =$ 10.56 GeV) to search for an electric dipole moment $d_e(q^2 = 0)$ at lower q^2. However the electric dipole moment arises from the same type of physics beyond the standard model as can be seen in figure 2 and so we need to evaluate the different sensitivities. The dependence of the observables differs by the ratio of the center of mass energy and the square root of the dipole moment [22].

$$\begin{aligned} < O^- > &\propto \frac{m_Z}{e} d(q^2 = m_Z) \\ < O^- > &\propto \frac{10.56}{e} \sqrt{d(q^2 = 0)} \end{aligned}$$

Using non-optimal observables it has been estimated that with 10^6 tau pairs at a B-factory we can achieve the same sensitivity as with 10^7 Z's at LEP [22]. This means that CLEO would currently need 2×10^6 tau pairs. CLEO currently has 4.2×10^6 tau pairs so it would be possible to make a competitive measurement.

4.2 CP violation in tau decay

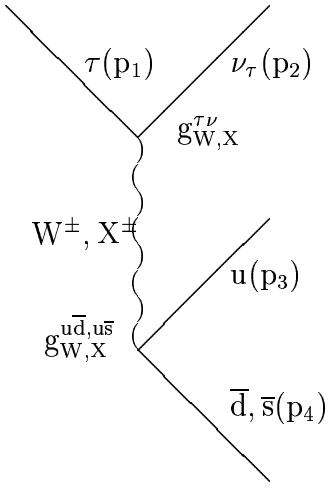

Figure 4: Definition of coupling constants and four momenta for tau decay via W or X boson. The four momenta refer to the final state particles (K, π) produced from the hadronization of the quarks

CP violation in tau decay has not been searched for previously. In order to observe CP violation we need to introduce an additional charged boson X with a CP violating coupling as in figure 4. CP violating effects are detectable in the interference of the two diagrams by comparing τ^+ to τ^- decays. In order that CPT is respected this can only occur if there is a relative CP even phase between the two. The only possible phase is the strong phase which arises from QCD final state interactions between quarks so that we only consider the semi-leptonic decays of the tau. The two quark possibilities are

$$\tau^- \to u\bar{d}\nu_\tau$$

$$\tau^- \to u\bar{s}\nu_\tau$$

The final state interaction arises from resonances in the final state and can be related to hadron scattering. In hadron scattering the incoming and outgoing particles are analyzed in terms of their component waves of a particular

angular momentum (S wave: l=0, P wave l=1 etc.) because the interaction proceeds through resonant states of a particular angular momentum. The amplitude is then proportional to [23]

$$\Sigma(2l+1)\eta_l e^{i\delta_l} P_l(cos\psi_{scat})$$

where P_l are the Legendre polynomials describing the angular distribution in terms of a scattering angle ψ_{scat} and each wave has amplitude $\mid \eta_l \mid$ and phase shift δ_l. At resonance the phase shift is $\pi/2$. The $u\overline{d}$ final state is experimentally observed to be dominated by the vector (l=1) ρ resonance and is Cabbibo favored ($br(\tau^- \to \rho^- \overline{\nu_\tau}) = 25.25 \pm 0.16\%$) [24] while the $u\overline{s}$ final state is experimentally observed to be dominated by the vector (l=1) K^* resonance and is Cabbibo suppressed ($br(\tau^- \to K^{*-} \overline{\nu_\tau}) = 1.28 \pm 0.08\%$) [24]. In order to have a different strong phase the interfering X boson must therefore be a scalar. There is then interference between the S wave final state from X exchange and P wave final state from W exchange. This interference results in detectable effects in the angular distribution which are different for τ^+ and τ^-. To show this we consider the diagram in figure 4. The CP even S,P wave strong phases are $\delta_{s,p}$ and the CP odd weak phase is θ. In each diagram the coupling constants are given by

$$\begin{aligned} g_W e^{i\delta_p} &= g_W^{\tau\nu} . g_W^{u\overline{d}} \\ g_X e^{i\delta_s} e^{i\theta} &= g_X^{\tau\nu} . g_X^{u\overline{d}} \end{aligned}$$

The width for τ^+ is then

$$\Gamma^+ = \frac{1}{2m_\tau}\frac{1}{(2\pi)^5}\int\frac{d^3p_2}{2E_2}\int\frac{d^3p_3}{2E_3}\int\frac{d^3p_4}{2E_4}\delta^4(p_1-p_2-p_3-p_4) \mid g_W e^{i\delta_p} A_W + g_X e^{i\delta_s} e^{i\theta} i A_X \mid^2$$

We are only interested in the interference term. If we denote the interfering part of the matrix element as M_{WX}

$$M_{WX} = \frac{1}{2m_\tau}\frac{1}{(2\pi)^5}\int\frac{d^3p_2}{2E_2}\int\frac{d^3p_3}{2E_3}\int\frac{d^3p_4}{2E_4}\delta^4(p_1-p_2-p_3-p_4) A_W A_X$$

then the width for the τ^+ and the CP conjugate τ^- will have interference terms:

$$\begin{aligned} \Gamma^+_{int} &= 2 g_w g_X cos(\delta_p - \delta_s - \theta) M_{WX} \\ \Gamma^-_{int} &= 2 g_w g_X cos(\delta_p - \delta_s + \theta) M_{WX} \end{aligned}$$

so that

$$\Gamma^{+}_{int} - \Gamma^{-}_{int} = 2 g_w g_X \sin(\delta_p - \delta_s) \sin\theta M_{WX}$$

There is no CP violation if $\theta = 0$ as expected. For a given θ the effect is maximal when $\sin(\delta_p - \delta_s) = 1$. The P wave amplitude is dominated by the resonant states ρ and K^*. At resonance the the phase shift is $\pi/2$ while the S wave phase shift is small since there is no observed scalar resonance so $\sin(\delta_p - \delta_s) \simeq 1$. The matrix elements above have been calculated in [25] [26]. Using the four-momenta assignments in figure 4 $p_i = (E_i, \vec{p_i})$:

$$A_W A_X = \mid f_1 \mid m_\tau (2(p_3 - p_4).p_1 - \frac{m_3^2 - m_4^2)}{(p_3 + p_4)^2}((p_3 + p_4)^2 + m_\tau^2)$$

$\mid f_1 \mid$ is the p-wave form factor (i.e Briet-Wigner for the resonance).In the hadronic rest frame $\vec{p_3} + \vec{p_4} = 0$ the matrix element reduces to a simple form

$$A_W A_X = \mid f_1 \mid 2m_\tau \mid \vec{p_3} - \vec{p_4} \mid\mid \vec{p_1} \mid \cos\alpha$$

where $\cos\alpha$ is the angle between the tau direction and either of the hadrons ($\vec{p_3} = -\vec{p_4}$). This difference in the interference terms is then proportional to the CP violating phase θ ,the coupling constants and the measurable angle α

$$\Gamma^{+}_{int} - \Gamma^{-}_{int} \propto g_w g_X sin\theta cos\alpha$$

The number of events is related to the width and the integrated luminosity

$$N = \Gamma . \int L dt$$

Hence we define an asymmetry

$$A_{cp} = \frac{N^+ - N^-}{N^+ + N^-} \propto g_w g_X sin\theta cos\alpha$$

$N^{\pm}$ is the number of $\tau^{\pm}$ events with angle $\cos\alpha$. The above holds for both the $u\overline{d}$ and $u\overline{s}$ final states. The quark final states hadronise via the strong interaction to form $\pi^{\pm}\pi^0$ and $K^0 h^{\pm}$ or $k^{\pm}\pi^0$ final states respectively where h is either a pion or kaon. However, there are some additional constraints on the magnitude of the CP violating effects that arises from consideration of Bose statistics and isospin conservation [25].

	I	I_3	S
u	1/2	1/2	1/2
d	1/2	-1/2	1/2
s	1/2	-1/2	1/2
π^+	1	1	0
π^0	1	0	0
π^-	1	-1	0
K_s^0	1/2	1/2	0

Table 2: Isospin and Spin assignments

The π^+ and π^0 are both spin-less bosons from table 2. The $(\pi^+\pi^0)$ final state must be symmetric under interchange since they can not interact electro-magnetically and are identical under the strong interaction (strong interaction conserves I not I_3). Conservation of angular momentum means that $S = 0$ X exchange results in an $L = 0$ final state. The symmetry under interchange is given by $(-1)^{L+I}$ so I must be even. Also since $I_3 = 1$ for the final state $I \neq 0$ hence $I = 2$.

The $u\overline{d}$ are produced in an $I = 1$ state so the hadronization process implies $\Delta I = 1$ which violates isospin conservation in strong interactions. However isospin can be violated by electro-magnetic decays and by the u and d mass difference at the level of a few percent. We therefore expect only a small s-wave contribution from the $\pi^{\pm}\pi^0$ final state to interfere with the p wave from W exchange.There is no equivalent argument for the $(u\overline{s})$ final state so CP violating effects are not suppressed in this mode.

5 Experimental Observables

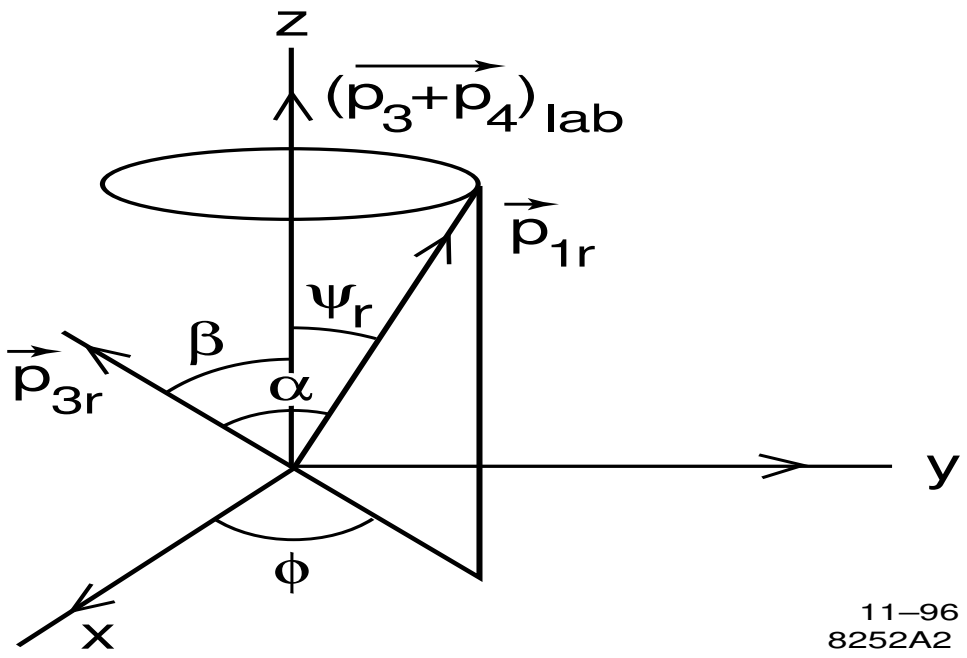

Figure 5: Definition of angles in the hadronic rest frame. $\vec{p_3} + \vec{p_4}$ is the direction of the lab frame viewed from the hadronic rest frame. The tau flight direction lies on a cone of angle ψ about this direction. The final state hadrons are back to back in this frame and make angle β with the lab frame direction. The angle between the hadrons and the tau flight direction is α.

In order to search for CP violation we need to measure the angle between one of the hadrons and the tau flight direction in the hadron rest frame in the decays.

$$\begin{aligned} \tau^{\pm} &\rightarrow \pi^{\pm}\pi^0\nu_\tau \\ \tau^{\pm} &\rightarrow k^{\pm}\pi^0\nu_\tau, K^0\pi^{\pm}\nu_\tau \end{aligned}$$

Figure 5 shows the experimental situation. We define a hadron vector $p_h = (E_h, \vec{p_h})$ to be the sum of the observed hadron energy-momentum $p_h = p_3 +$

p_4. The mass of the hadron vector is given by $m_h = p_h^2$. In the hadron rest frame $\vec{p_h} = 0$ the direction of the laboratory $\hat{p_{lab}}$ as viewed from this frame is $-\hat{p_h}$. The tau flight direction lies on a cone of angle ψ about $\hat{p_{lab}}$. This uncertainty in the tau direction corresponds to the loss of information from the unmeasured neutrino. The angle is given in terms of measurable quantities by [27]:

$$\cos\psi = \frac{x(m_\tau^2 + m_h^2) - 2m_h^2}{(m_\tau^2 + m_h^2)\sqrt{x^2 - 4m_h^2/s}}$$

where $x = 2\frac{E_h^{lab}}{\sqrt{s}}$ and $\sqrt{s}$ is the center of mass energy. The angle β is similarly measurable but the angle of interest α is unmeasurable due to the uncertainty in the tau flight direction. However we can express α in terms of ψ,β and the azimuthal angle ϕ [28].

$$\cos\alpha = \cos\beta\cos\psi + \sin\beta\sin\psi\cos\phi$$

In calculating the width from the matrix element we integrate over the unmeasured angle ϕ so that the second term above vanishes

$$\int_0^{2\pi} \cos\phi d\phi = 0$$

This means that in the expression for the asymmetry A_{cp} we can replace $\cos\alpha$ by $\cos\beta\cos\psi$ to give

$$A_{cp} = \frac{N^+ - N^-}{N^+ + N^-} \propto g_w g_X \sin\theta\cos\beta\cos\psi$$

We can test for CP violation by measuring two angles in the hadronic decay of the tau. These angles can be best measured if all the final state particles are charged since we can exploit the precision of the tracking chambers. This occurs in the decays containing a K^0 since the K^0 is 50 % K_s^0 and 50 % K_L^0. While the K_L^0 is undetectable the K_s^0 decays to two charged pions after traveling a short distance in the detector.

$$\tau^\pm \to K^0\pi^\pm \qquad K^0 \to \pi^+\pi^-$$

The angles can be measured but less accurately in decays containing a π^0. Note that the tau direction can be inferred to within a two-fold ambiguity if

both taus in the event decay hadronically since we can intersect the two tau flight direction cones and the ambiguity can be resolved by a precision vertex detector [17]. However in this case there are lower statistics since we require hadronic decays of both taus in the event rather than one. In addition most of the hadronic decays contain a π^0 which are not detected in the tracking chambers so the angles are poorly measured.

6 Experimental Constraints

Since this is the first ever search for CP violation in lepton decay there are no explicit constraints. However there are constraints on the magnitude of additional couplings in tau decays provided by the recent CLEO Michel parameter analysis [18]. In this analysis the most general possible matrix element (scalar,vector or tensor couplings to right or left handed leptons) is fit to all measurable parameters of $\tau^{\pm}$ decay. The coupling strengths are parameterized in terms of the standard model coupling (i.e $g = g_x/g_w$ in our notation). Figure 6 shows the allowed ranges of g. Note that values as high as $g = 1$ are allowed for scalar and tensor couplings. The constraints are on the magnitude of the couplings and the analysis is insensitive to the phase of the coupling (i.e CP violation).

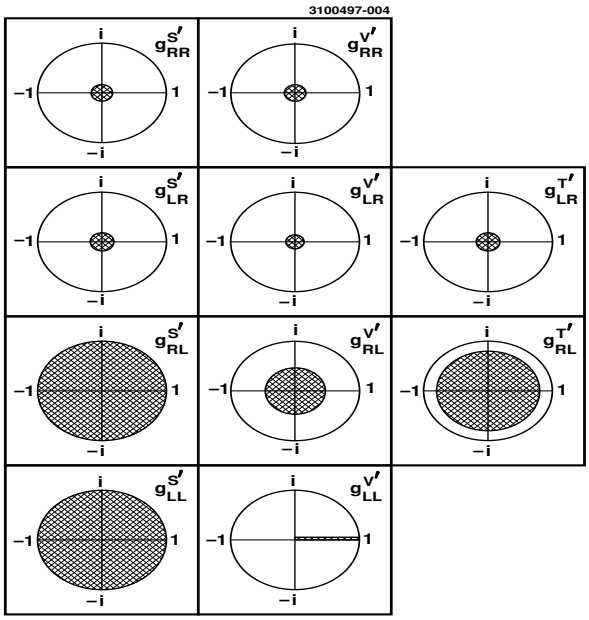

FIG. 4. 90% confidence limits on the reduced coupling constants $g^{\gamma'}_{e\mu} = g^{\gamma}_{e\mu}/max(g^{\gamma}_{e\mu})$.

Figure 6: Shaded areas show allowed magnitude of coupling constants for scalar,vector or tensor couplings to right and left handed tau decays. The couplings are measured in standard model units $g = g_x/g_w$

7 Experimental Signature

The most favorable channel to search for CP violation in tau decay is

$$\tau^{\pm} \to K^0_s \pi^{\pm} \nu_{\tau} \qquad K^0_s \to \pi^+ \pi^-$$

- The strong phases for S and P wave decay make it possible to observe CP violation in this channel.
- There is no suppression due to isospin violation as in the $\tau \to \pi^{\pm}\pi^0\nu_\tau$ channel.
- The standard model decay is dominated by the $K^{*\pm}(892)$ resonance meaning that there is a maximal phase shift between S and P wave final states so the sensitivity to CP violation is maximal.
- The final state is three charged pions allowing accurate measurement of the charged tracks and reconstruction of the angles β and α.
- The decay of the k_s^0 to two charged pions provides a very distinctive signature to identify these decays.

The single disadvantage is the low branching ratio: CLEO currently has a

	Branching ratio (%)
$\tau \to K^0\pi^{\pm}\nu_\tau$	0.70 ± 0.10
$K^0 \to K_s^0$	50.0
$K_s^0 \to \pi^+\pi^-$	68.6 ± 0.3
Product	0.24 ± 0.04

data set of 4.42×10^6 tau pairs so that there will be a maximum of approximately 21000 signal events in our dataset.

To demonstrate the experimental signature of CP violation we use a modified version of the TAUOLA monte-carlo [29]. It has been modified to include a scalar or pseudoscalar coupling in the hadronic decay of the tau [30]. The scalar form factor is set to unity i.e non-resonant decay. The input parameter is the imaginary part of the additional coupling in units of the standard model $Im(g) = Im(g_X e^{i\theta}/g_W)$. In figure 7 we plot the product of the angles defined above $(\cos\beta\cos\psi)$ for truth table monte-carlo for τ^+ and for τ^-. In this case we have chosen a maximal value of $Im(g) = 1$ (i.e$g_X = g_W, \theta = \pi/2$). Also shown for comparison is the case where the tau flight direction is measured $(\cos\alpha)$.

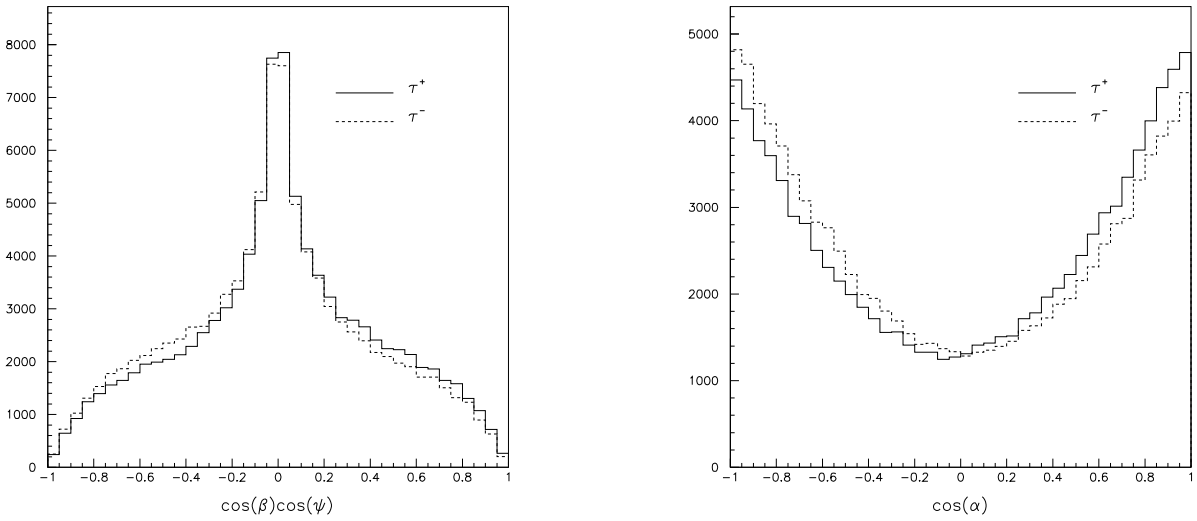

Figure 7: The different angular dependence for τ^+ and τ^+due to interference of the standard model and X boson amplitudes. This plot uses truth table monte-carlo (Im(g)=1) and shows both the case where the tau flight direction is unmeasured ($\cos\beta\cos\alpha$) and measured $\cos\alpha$.

The asymmetries are small even in this maximal case. The derived asymmetry A_{cp} is also shown. For simplicity and to get the most statistics in one bin we divide the asymmetry into two cases

$$\begin{aligned} A^+_{cp} &= A_{cp} \qquad \cos\beta\cos\psi, \cos\alpha > 0.0 \\ A^-_{cp} &= A_{cp} \qquad \cos\beta\cos\psi, \cos\alpha < 0.0 \end{aligned}$$

The asymmetries are tabulated below for figure 7. It is higher for the case where we measure accurately the tau flight direction. However, since both taus in the event are required to decay hadronically we have only half of the statistics (see table 3) and the flight direction will be measured poorly. We only consider the case in which the flight direction is not measured.

	$\cos\beta\cos\psi$	$\cos\alpha$
$A_{cp}^{+}(\%)$	$(3.3 \pm 0.3).Im(g)$	$(5.4 \pm 0.3).Im(g)$
$A_{cp}^{-}(\%)$	$(-3.3 \pm 0.3).Im(g)$	$(-5.4 \pm 0.3).Im(g)$

8 Dataset

In e^+ e^- collisions at $\sqrt{s} = 10.6\ GeV$ we produce continuum $q\overline{q}$ pairs ($q = uds$), $c\overline{c}$, $b\overline{b}$ and $\tau^+\tau^-$. We define cuts to give a pure sample of $\tau^+\tau^-$ and further to separate out from the τ sample the decay

$$\tau^{\pm} \to K^0 h^{\pm} \nu_\tau \qquad K^0 \to \pi^+\pi^-$$

The signal tau decay recoils against the "tag" tau. We have used a standard one prong tag. Table 3 lists the dominant modes which contribute to the tags.

	Branching ratio (%)
$\tau \to e\nu\overline{\nu}$	17.83 ± 0.08
$\tau \to \mu\nu\overline{\nu}$	17.35 ± 0.10
$\tau \to h^{\pm}\nu$	12.03 ± 0.14
$\tau \to h^{\pm}h^0\nu$	25.76 ± 0.15
Total	72.97 ± 0.24

Table 3: tag modes used and branching ratio

The total integrated luminosity of the data set is 4.78 fb^{-1} (4s1-4sG) which corresponds to 4.41×10^6 $\tau^+\tau^-$ pairs . The cuts are also standard CLEO tau analysis cuts that have been used in previous analysis. In particular the cuts are essentially those used for previous $\tau \to K_s^0 h^- \nu_\tau$ [34] but with slightly lower thresholds to increase acceptance.

1. **Track Multiplicity Cut.** $N_{track} = 4$. $\Sigma_{tracks} Q = 0$. The tracks are required to pass standard quality cuts (TRKMAN [31]),KINCD.ge.0,DBCD¡0.01, lie in a fiducial region of tracking coverage ($|\cos\theta_{track}| < 0.90$) and have

transverse momentum greater than 0.025 beam energy. The tau decays to an odd number of charged tracks. The signal decay has 3 charged tracks in the final state and the tag modes all have one charged track to give a total of 4 with no net charge. Events with conversions as identified by GCFIND are vetoed.

2. **Tag track isolation cut.** $\Theta_{isolation} > 90^0$. At least one of the tracks must be separated from the other three tracks by greater than 90^o, have scaled transverse momentum $p_t/E_{beam} > 0.05$ and lie in a fiducial region of good tracking $|\cos\theta| < 0.80$. The taus ($m_{tau} = 1.777GeV$) are produced above threshold at $\sqrt{s} > 10.56GeV$ and so recoil against each other in a jet-like topology which allows the event to be divided into a tag hemisphere and a decay hemisphere. The isolation cut identifies the tag track.

3. **Find K_s^0 secondary vertex** Require a displaced secondary vertex on decay side. We use the loose cuts for the VFND algorithm as in reference [34]. The K_s^0 travels several millimeters on average before decaying into two charged pions.

4. **π^0 Veto** We allow a maximum of one π^0 in the tag hemisphere to include rho tags. The two photon clusters are required to have energy greater than 100 MeV, lie in the tag hemisphere, be in the good barrel region of the calorimeter ($|\cos\theta| < 0.71$), be unmatched to a track (CDCC match types 1,2 or 4,5), not lie within 30 cm of a track, and form an invariant mass within 3 sigma of the π^0 mass. We veto an event with a π^0 in the signal hemisphere. The π^0 is defined as above except that both clusters must be in the signal hemisphere and have energy greater than 60 MeV (A lower threshold is used since it is a veto). This cut reduces continuum and tau feeddown backgrounds.

5. **Unmatched Photon Veto** We veto events with an unmatched photon of energy greater than 100 MeV on the signal side or 300 MeV on the tag side. The photon must be unmatched to a track (CDCC match type 1,2 or 4,5), not lie within 30 cm of a track, pass the 1% e9e25 photon cuts, have $|\cos\theta| < 0.85$ and not be used in the π^0 for the rho tag. The higher threshold on the tag side is to increase acceptance of the rho tag

modes where one of the photons from the π^0 has been misreconstructed. This cut reduces continuum and tau feeddown backgrounds.

6. **Unmatched Cluster Veto** We veto events with an unmatched calorimeter cluster of energy greater than 350 MeV on the decay side. The cluster must be unmatched to a track (CDCC match type 1,2 or 4,5), have $\mid \cos\theta \mid < 0.85$ and not be used in the $\pi 0$ for the rho tag. This is to remove events with K_L^0 in the decay.

7. **Global Event Cuts.** $0.7 < E_{visible}/E_{beam} < 1.6$. $p_t^{\vec{miss}} > 0.03$. $\mid \cos\theta^{miss} \mid < 0.95$. The visible energy $E_{visible}$ is given by the scalar sum of the track momentum over all tracks and all calorimeter clusters unmatched to a track. $E_{visible} = \Sigma_{tracks} \mid \vec{p} \mid + \Sigma_{unmatched\ clusters} \mid E \mid$. The missing transverse momentum vector $p_t^{\vec{miss}}$ is the transverse component (normal to beam line) of the vector sum over all tracks and unmatched clusters $p_t^{\vec{miss}} = \Sigma_{tracks}(\vec{p_x} + \vec{p_y}) + \Sigma_{unmatched\ clusters}(E_x + E_y)$. θ^{miss} is the polar angle of the missing energy vector relative to the beamline. These cuts exploit the fact that there are two neutrinos which are undetected in the event and hence the total visible energy is less than twice the beam energy and a directional imbalance corresponding to average direction of the neutrinos. The lower bound on $E_{visible}$ and the θ^{miss} cut is to veto two photon events where most of the energy goes down the beam-pipe.

8 **Trigger and Skim Requirements** Require all events to pass the level 2 and level 3 trigger.

9 **Skim Requirements** Require all events to pass the standard tau skim cuts (TAUSKM).

10. **Require Invariant mass of secondary vertex consistent with K_s^0** . We perform an vertex constrained fit for the two tracks in the displaced secondary vertex and require the invariant mass be within 20 MeV of the true K_s^0 mass. The K_s^0 is required to travel at least 5mm from the interaction point before decaying.

Table 4 lists the efficiencies for each cut and the asymmetry after each. We use the modified TAUOLA event generator with Im(g)=1 and assuming a

Cut #	Cut	Efficiency %	A_{cp}^{-} %	A_{cp}^{+} %
0	No cuts	-	-3.3 ± 0.3	3.3 ± 0.3
1	track multiplicity	53.7 ± 0.1	-2.8 ± 0.4	2.7 ± 0.4
2	tag track isolation	75.5 ± 0.1	-2.8 ± 0.4	2.7 ± 0.4
3	K_s^0 Vertex	63.8 ± 0.3	-2.8 ± 0.4	2.7 ± 0.4
4	π^0 veto	93.6 ± 0.4	-2.9 ± 0.4	2.8 ± 0.4
5	Unmatched photon veto	69.6 ± 0.3	-4.0 ± 0.5	2.5 ± 0.5
6	Unmatched cluster veto	92.4 ± 0.5	-4.1 ± 0.5	2.4 ± 0.5
7	Global Event	78.8 ± 0.4	-3.8 ± 0.5	3.0 ± 0.5
8	L2 and L3 trigger	97.6 ± 0.5	-3.9 ± 0.6	3.1 ± 0.5
9	Tau skim	92.2 ± 0.5	-3.7 ± 0.6	3.1 ± 0.6
10	K_S^0 mass	94.0 ± 0.5	-3.6 ± 0.6	3.0 ± 0.6
-	All Cuts	10.4 ± 0.7	-3.6 ± 0.6	3.0 ± 0.6

Table 4: Cut efficiencies and asymmetry after each cut. The cuts are sequential so that for instance the efficiency and asymmetry for cut 3 assumes cut 1 and 2 have already been made. The TAUOLA event generator and GEANT detector simulation are used with a sample of 400000 events with Im(g)=1. The errors are statistical

strong phase difference of $\pi/2$. The events are then passed through the full GEANT detector simulation. The cuts are CP symmetric and the asymmetry is not degraded to within the statistical accuracy of the monte-carlo. Figure 8 shows the angular distributions for τ^+ and τ^- after all cuts. The statistics in the region $\cos\beta\cos\psi < 0$ are degraded because this region is more heavily populated by the lower momentum tracks from the tau decay which are removed by cut 2. The experimentally observable asymmetry is then in general given in terms of the coupling strength Im(g) by

$$A_{cp}^{\pm}(\%) = \pm 3.3.Im(g)$$

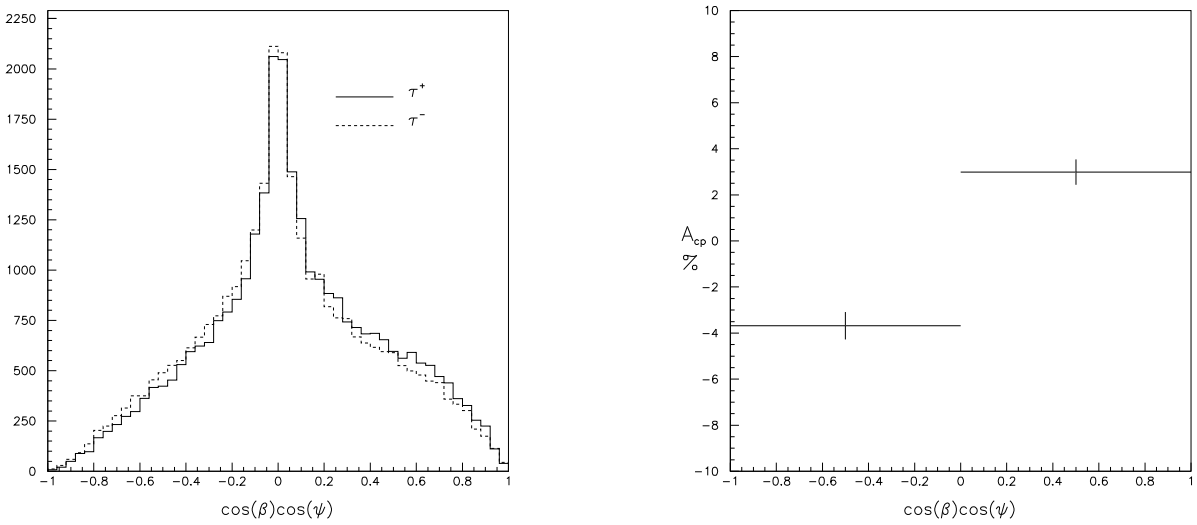

Figure 8: The different angular dependence for τ^+ and τ^+due to interference of the standard model and addition X boson amplitudes after all analysis cuts. The TAUOLA event generator with Im(g)=1 is used and the events are passed through the full geant detector simulation and required to pass all cuts. Also shown is the derived asymmetry A_{cp} .

The approximate number of events expected in the sample is given by

$$N_{\tau\to K^0_s\pi\nu} = 2.0.\sigma_{\tau^+\tau^-}.\int Ldt.B_{\tau\to K^0_s\pi\nu}\epsilon_{cuts} = 2201 \pm 241$$

where

$$\begin{aligned} 2.\sigma_{\tau^+\tau^-}.\int Ldt &= 2 \times 4.41 \pm 0.05 \times 10^6 \\ B_{\tau\to K^0_s\pi\nu} &= 0.0024 \pm 0.0003 \\ \epsilon_{cuts} &= 0.104 \pm 0.001 \end{aligned}$$

9 Results

Figure 9 shows the invariant mass of the K_s^0 for events passing all cuts(1-5) except the cut on the mass itself. It can be seen that a reasonably pure sample of events are selected.

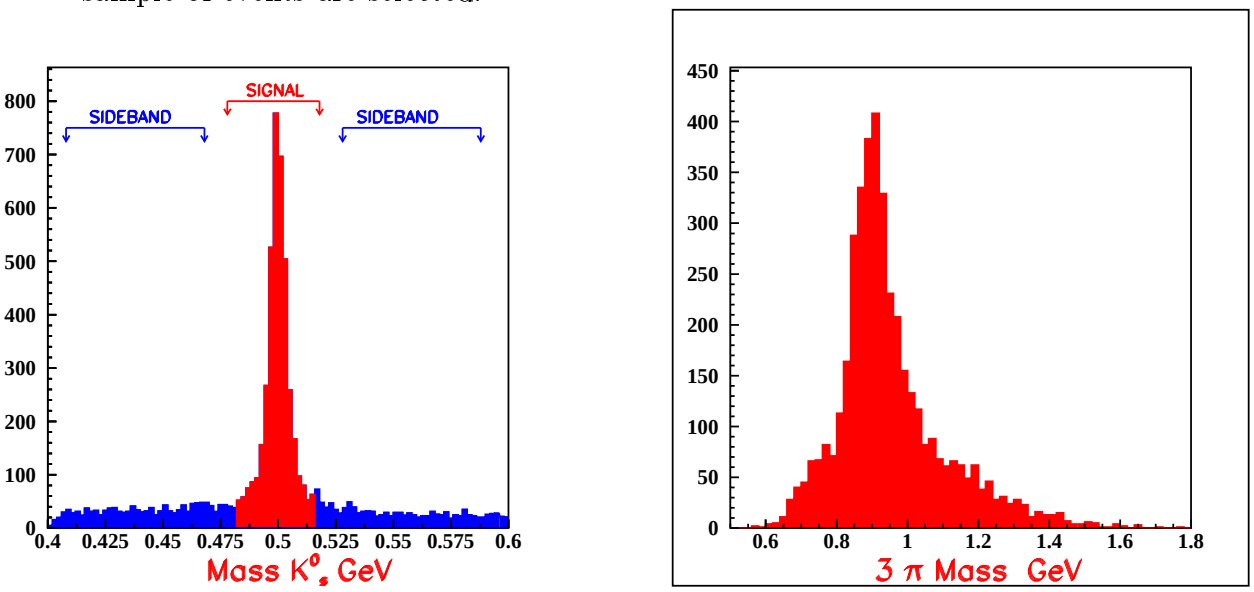

Figure 9: Invariant mass of K_s^0 candidate in data after all cuts with signal and sideband regions are denoted. Also shown is the 3 pi invariant mass. The $K^*(892)$ is clearly visible

The $\cos\beta\cos\psi$ distribution for τ^+ and τ^- after all cuts is shown in figure 10. Also shown is the derived asymmetry. A 3.5 sigma non-zero asymmetry is observed. Errors are statistical.

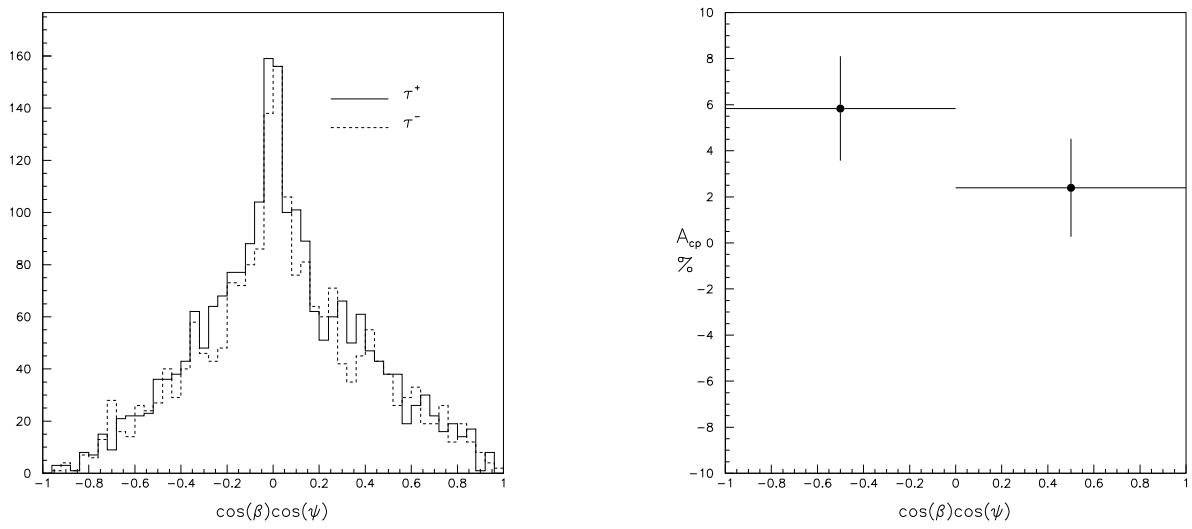

Figure 10: The angular dependence for τ^+ and τ^+ for events passing all cuts in data. The derived asymmetry is also shown. Errors are statistical.

$A_{cp}^{-}(\%)$	$A_{cp}^{+}(\%)$
5.8 ± 2.3	2.4 ± 2.1

The values of the measured asymmetry are given in table 9. The errors are purely statistical. The total number of events in the signal region is 4169 which is considerably larger than the predicted 2201 $K^0\pi\nu_\tau$ due to backgrounds.

10 Backgrounds

Table 5 lists the estimated backgrounds in the sample. The estimate is made using a large MC data sample of generic tau decays (10.5×10^6 events) and continuum ($q\overline{q}$) (11.4×10^6 events). The standard TAUOLA event

Tau Mode	Br.	ϵ %	N_{Sig}	N_{sig}^{total} %	N_{Side}	N_{side}^{total} %
$K_S^0(\pi^+\pi^-)\pi^-\nu_\tau$	0.24 ± 0.04	10.4±0.12	2201±241	52.5±5.7	99± 12	4.3±0.5
$K^0K^-\nu_\tau$	0.15 ± 0.04	3.9±0.12	520±241	12.4±3.6	22± 6	1.0±0.3
$a1\nu_\tau$	8.8 ± 0.1	0.057±0.002	442±14	10.6±0.3	1420±31	61.7±1.3
$K^0\pi^-\pi 0\nu_\tau$	0.41 ±0.1	0.76±0.03	276±69	6.6±1.6	13±4	0.6±0.2
$K^0\overline{K0}\pi^-\nu_\tau$	0.10 ±0.03	2.63±0.08	232±74	5.5±1.8	7±3	0.3±0.1
$K^0K^-\pi 0\nu_\tau$	0.13 ±0.03	1.2 ±0.06	128±34	3.1±0.8	6±2	0.3±0.1
$\pi^+\pi^-\pi^-\pi 0\nu_\tau$	4.5 ±0.1	0.03±0.002	119±7	2.8±0.2	386±15	16.7±0.7
$K^+\pi^+\pi^-\nu_\tau$	0.42 ±0.18	0.09±0.01	35±15	0.8±0.3	100±43	4.3±0.7
others	-	-	51±11	1.2±0.2	164±52	7.1±2.35
$q\overline{q}$	-	0.0014±0.0001	186±13	4.5±0.2	84±9	3.7±0.3
Total MC	-	-	4190±304	100.0±7.0	2301±74	100.0±3.2
Total Data	-	-	4169	-	2081	-

Table 5: Single and sideband composition by mode. Branching ratios taken from PDG and efficiencies computed with standard TAUOLA monte carlo and GEANT detector simulation.

generator and full GEANT detector simulation are used and the events are required to pass all cuts. CP violating effects may exist in the backgrounds and we need to assess the magnitude. There are two effects that may suppress the asymmetry. The first is specific to a Higgs type scalar. Any asymmetry deriving from a $\tau^- \to \overline{u}d\nu_\tau$ coupling will be suppressed relative to a $\tau^- \to \overline{u}s\nu_\tau$ coupling by a factor $m_d/m_s \simeq 1/20$ due to the mass dependence of the coupling. Secondly the asymmetry derives from interference of s wave scalar exchange with p wave vector exchange. If however the standard model decay is s wave then the the interference effect vanishes. For instance in the case of $\tau^- \to a1\nu_\tau \to \rho\pi\nu_\tau \to \pi\pi\pi\nu_\tau$ the $\rho\pi$ system is produced in an s wave configuration while the rho decays in a P wave configuration. In our analysis we reconstruct a two body decay so that 50 % of the time the two body system is reconstructed as s wave and the rest of the time the reconstruction is incorrect and we get a diluted S wave contribution. The net effect is to diminish the experimental sensitivity by a factor of 4-5. A similar argument applies for each of the other three body background modes. For each of the background modes we tabulate the expected suppression factor. We assume

that the continuum exhibits no CP violation.

Tau Mode	Mass Suppression	P wave Dilution	Overall Suppression
$K^0_S(\pi^+\pi^-)\pi^-\nu_\tau$	1	1	1
$K^0K^-\nu_\tau$	1/20	1	1/20
$a1\nu_\tau$	1/20	1/4 ($a1 \to \rho\pi$)	1/80
$K0\pi^-\pi0\nu_\tau$	1	1/4 ($K_1 \to K\rho, K^*\pi$)	1/4
$K0\overline{K0}\pi^-\nu_\tau$	1/20	1/4 ($\rho^{'} \to K^*K0$)	1/80
$K0K^-\pi0\nu_\tau$	1/20		1/20
$\pi^+\pi^-\pi^-\pi0\nu_\tau$	1/20		1/20
$K^+\pi^+\pi^-\nu_\tau$	1	1/4 ($K_1 \to K\rho, K^*\pi$)	1/4
others	-	-	-
$q\overline{q}$	-	-	

Table 6: Suppression factors for each mode. The suppression factor is the maxminal CP violation expected realtive to the signal mode.

The effective contribution of each mode to an asymmetry measurement is discussed in the next section.

11 Systematics

The observed asymmetry for a particular mode is given in terms of the efficiencies ϵ and the cross-sections σ

$$A_{observed} = \frac{N(+) - N(-)}{N(+) + N_i(-)} = \frac{\epsilon(+)\sigma(+) - \epsilon(+)\sigma(+)}{\epsilon(+)\sigma(+) + \epsilon(+)\sigma(+)}$$

An asymmetry can be observed if there is either a real physical asymmetry $\sigma(+) \neq \sigma(-)$ or a detector induced asymmetry $\epsilon(+) \neq \epsilon(-)$. Thus systematic differences in the detection efficiencies for positive and negative taus can fake CP violation. There are a variety of effects that may cause such differences. These are discussed in detail in appendix C.

To understand quantitatively how these effects enter into the observed asymmetry let

$$\sigma(-) = (1 - \alpha)\sigma(+)$$

and

$$\epsilon(-) = (1-\beta)\epsilon(+)$$

Then

$$A_{observed} = \frac{1-(1-\beta)(1-\alpha)}{1+(1-\beta)(1-\alpha)}$$

If there is no physical asymmetry then $\alpha = 0$ and only a detector induced asymmetry is observed

$$A_{observed} = A_{detector} = \frac{\beta}{2-\beta}$$

Similarly if there are no detector induced effects $\beta = 0$ and only a physical CP asymmetry is observed

$$A_{observed} = A_{cp} = \frac{\alpha}{2-\alpha}$$

$A_{observed}$ can be expressed in terms of the pure detector asymmetry and the pure CP asymmetry as follows

$$A_{observed} = \frac{1-(1-\beta)(1-\alpha)}{1+(1-\beta)(1-\alpha)} = \frac{\alpha+\beta-\alpha\beta}{2-\alpha-\beta+\alpha\beta} \simeq \frac{\alpha+\beta}{2-\alpha-\beta}$$

$$A_{detector} + A_{cp} = \frac{\beta}{2-\beta} + \frac{\alpha}{2-\alpha} = \frac{\alpha+\beta-\alpha\beta}{2-\alpha-\beta+\frac{\alpha\beta}{2}} \simeq \frac{\alpha+\beta}{2-\alpha-\beta}$$

Where we have assumed that the asymmetries are small so that $\alpha \ll 1$,$\beta \ll 1$ and $\alpha\beta$ can be neglected. Then

$$A_{observed} = A_{cp} + A_{detector}$$

This then implies that we can use a control sample where no CP violation is expected to estimate the detector effects and then subtract them off from the observed asymmetries to extract the true CP asymmetry. Such a sample is provided by the K^0_s sidebands but the situation is slightly complicated by the presence of backgrounds. We now consider quantitatively how the asymmetries are affected by backgrounds. Suppose in a measurement we observe a sum of different modes. Each mode constitutes a fraction f_i of the total sample. If the asymmetry for a particular mode i is

$$A^i = \frac{N(+)-N(-)}{N(+)+N(-)} = \frac{d^i}{s^i}$$

We measure the asymmetry for a sample containing several different modes

$$A = \frac{D}{S} = \frac{\Sigma^i d^i}{\Sigma^i s^i}$$

The observed asymmetry can be related to the asymmetries of the individual modes

$$A = \frac{\Sigma^i d^i}{S} = \Sigma_i \frac{d^i}{s^i}\frac{s^i}{S} = \Sigma^i f^i A^i$$

If a sample contains for example 80 % of a mode with a CP asymmetry of A_{cp} and 20 % background with no CP violating asymmetry then observed asymmetry is diluted $A_{observed} = 0.8A_{cp}$. The most general expression for an asymmetry is then

$$A_{observed} = \Sigma_{i=modes} f^i (A^i_{CP} + A^i_{detector})$$

We expect that the detector asymmetries for each different mode should be the same since each mode in a sample occupies the same phase space and we expect the detector efficiencies to be functions of the the particle four vectors.

$$A_{observed} = A_{detector} + \Sigma_{i=modes} f^i A^i_{CP}$$

If we now make an asymmetry measurement for both signal and sideband regions

$$A(sig)_{observed} = A_{detector} + \Sigma_{i=modes} f(sig)^i A^i_{CP}$$
$$A(side)_{observed} = A_{detector} + \Sigma_{i=modes} f(side)^i A^i_{CP}$$

Subtracting

$$\Sigma_{i=modes}(f(sig)^i - f(side)^i)A^i_{CP} = A(sig)_{observed} - A(side)_{observed}$$

We can thus use the sidebands to subtract out the detector effects which are difficult to model and the monte-carlo to estimate the signal and sideband compositions which allows us to extract a CP asymmetry measurement.

12 Final asymmetry measurement

Tau Mode	α	F_{sig} %	F_{side} %	$(F_{sig} - F_{side}).\alpha$ %
$K^0_S(\pi^+\pi^-)\pi^-\nu_\tau$	1	52.5 ± 5.7	4.3 ± 0.5	48.2 ± 5.7
$K^0K^-\nu_\tau$	1/20	12.4 ± 3.6	0.9 ± 0.3	0.57 ± 0.2
$a1\nu_\tau$	1/80	10.6 ± 0.3	62.0 ± 1.3	-0.64 ± 0.02
$K^0\pi^-\pi 0\nu_\tau$	1/4	6.6 ± 1.6	0.6 ± 0.2	1.50 ± 0.4
$K^0\overline{K^0}\pi^-\nu_\tau$	1/80	5.5 ± 1.8	0.3 ± 0.1	0.07 ± 0.02
$K^0K^-\pi^0\nu_\tau$	1/20	3.0 ± 0.8	0.3 ± 0.1	0.14 ± 0.04
$\pi^+\pi^-\pi^-\pi^0\nu_\tau$	1/20	2.8 ± 0.2	16.7 ± 0.7	-0.7 ± 0.04
$K^+\pi^+\pi^-\nu_\tau$	1/4	0.8 ± 0.3	4.3 ± 0.7	-0.9 ± 0.21
others	0	1.2 ± 0.2	7.1 ± 1.7	0
$q\overline{q}$	0	4.4 ± 0.3	3.7 ± 0.3	0
Total	-	$100. \pm 7.0$	$100. \pm 3.2$	48.2 ± 6.1

Table 7: Relative asymmetry expected in the sample after subtracting the measured asymmetry from the sidebands. The total in the last column is the overall dilution factor for the asymmetry

Table 7 indicates the relative weights of the asymmetry expected in the sample if we measure the asymmetry in the sidebands and subtract this from the signal asymmetry. It indicates that to a good approximation if there is a true physics asymmetry it should be heavily suppressed in the sidebands and that the backgrounds in the signal region serve to dilute the asymmetry rather than add to it. The sidebands are dominated by the $\tau^- \to \pi^-\pi^+\pi^-\nu$ mode with mismeasured tracks. We can cross-check any assumptions about the possibility of CP violation in this mode by checking in data. In appendix D we measure the asymmetry of this mode in a pure high statistics sample. The asymmetry is zero within statistical errors indicating no evidence of CP violation.

Figure 11 shows the measured asymmetries for the signal and sideband samples. Also shown is the asymmetry after the sideband has been subtracted out.

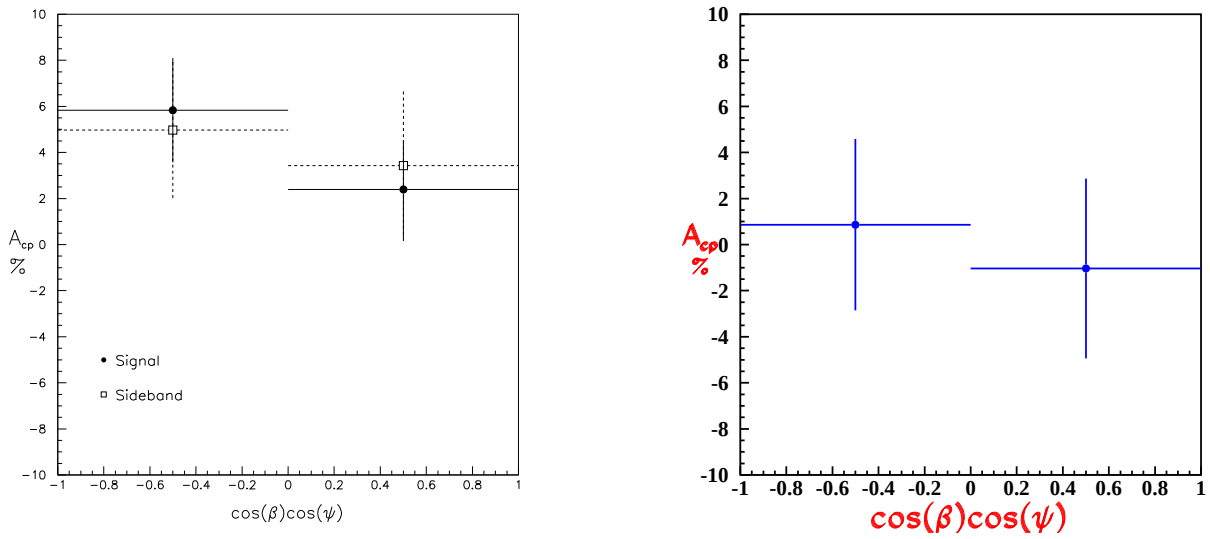

Figure 11: The asymmetry for signal and sideband data. Also shown is the sideband subtracted asymmetry.

	$A_{cp}^{-}(\%)$	$A_{cp}^{+}(\%)$
Signal	5.8 ± 2.3	2.4 ± 2.1
Sideband	4.9 ± 3.0	3.4 ± 3.3
Signal-sideband	0.9 ± 3.8	-1.0 ± 3.9

After sideband subtraction there is no statistical evidence for any asymmetry. The common asymmetry in the signal and sideband region is either a statitical fluctuation of the entire sample or a detector effect but can not be attributed to any CP violating effect.

13 Cut Sensitivity

To check that the analysis is stable with respect to changes in cuts we tabulate the measured asymmetry in signal, sideband and signal-sideband for a range of values about the nominal. The cut number used in section 6 is given for reference to a detailed description of the cut. The analysis is shown to be stable with respect to these changes.

13.1 Photon Veto Energy (Decay Side) - Cut 5

Energy (MeV)	Signal		Sideband		Signal-Sideband	
	$A_{cp}^{+}(\%)$	A_{cp}^{-} (%)	A_{cp}^{+} (%)	A_{cp}^{-} (%)	A_{cp}^{+} (%)	A_{cp}^{-} (%)
60	6.0 ± 2.4	2.3 ± 2.2	5.1 ± 3.1	3.8 ± 3.5	0.9 ± 3.9	-1.5 ± 4.1
80	6.1 ± 2.3	2.1 ± 2.2	4.6 ± 3.0	4.2 ± 3.4	1.6 ± 3.8	-2.1 ± 4.0
100(nominal)	5.8 ± 2.3	2.4 ± 2.1	5.0 ± 3.0	3.4 ± 3.3	0.9 ± 3.8	-1.0 ± 3.9
150	5.6 ± 2.7	1.8 ± 2.0	5.5 ± 2.8	1.7 ± 3.1	0.1 ± 3.5	0.1 ± 3.7
200	4.5 ± 2.1	2.3 ± 2.0	7.0 ± 2.7	1.0 ± 3.0	-2.5 ± 3.4	1.3 ± 3.6
350	3.9 ± 2.0	2.4 ± 1.8	5.5 ± 2.6	2.3 ± 2.8	-1.7 ± 3.2	0.1 ± 3.4

13.2 Isolated Photon Veto Energy (Tag Side) - Cut 5

Energy (MeV)	Signal		Sideband		Signal-Sideband	
	$A_{cp}^{+}(\%)$	A_{cp}^{-} (%)	A_{cp}^{+} (%)	A_{cp}^{-} (%)	A_{cp}^{+} (%)	A_{cp}^{-} (%)
60	8.0 ± 2.5	3.0 ± 2.3	7.2 ± 3.2	3.3 ± 3.6	1.1 ± 4.0	-0.3 ± 4.3
100	7.5 ± 2.4	3.0 ± 2.3	5.3 ± 3.1	3.6 ± 3.5	2.3 ± 3.9	-0.6 ± 4.1
200	6.8 ± 2.3	2.9 ± 2.2	4.4 ± 3.0	3.9 ± 3.4	2.4 ± 3.8	-1.0 ± 4.0
300(nominal)	5.8 ± 2.3	2.4 ± 2.1	5.0 ± 3.0	3.4 ± 3.3	0.9 ± 3.8	-1.0 ± 3.9
400	5.5 ± 2.2	3.1 ± 2.1	4.2 ± 2.9	3.1 ± 3.2	1.3 ± 3.6	0.0 ± 3.8
500	5.9 ± 2.2	3.1 ± 2.0	3.5 ± 2.8	3.0 ± 3.2	2.4 ± 3.6	0.0 ± 3.8

13.3 Cluster Veto Energy (Decay Side) - Cut 6

Energy (MeV)	Signal		Sideband		Signal-Sideband	
	$A_{cp}^{+}(\%)$	A_{cp}^{-} (%)	A_{cp}^{+} (%)	A_{cp}^{-} (%)	A_{cp}^{+} (%)	A_{cp}^{-} (%)
60	4.1 ± 2.5	0.2 ± 2.4	3.4 ± 3.3	5.4 ± 3.7	0.7 ± 4.2	-5.2 ± 4.4
100	4.7 ± 2.4	1.1 ± 2.2	4.5 ± 3.2	5.2 ± 3.5	0.3 ± 3.9	-4.1 ± 4.1
200	5.1 ± 2.3	1.7 ± 2.2	5.2 ± 3.0	3.9 ± 3.3	-0.1 ± 3.8	-2.0 ± 3.9
350(nominal)	5.8 ± 2.3	2.4 ± 2.1	5.0 ± 3.0	3.4 ± 3.3	0.9 ± 3.8	-1.0 ± 3.9
500	5.8 ± 2.2	2.3 ± 2.1	4.9 ± 2.9	3.6 ± 3.2	0.9 ± 3.7	-1.2 ± 3.9
700	5.8 ± 2.3	2.2 ± 2.1	4.4 ± 2.9	3.4 ± 3.2	1.4 ± 3.2	-1.2 ± 3.8

13.4 Photon Veto track shower distance - Cut 5

Distance (cm)	Signal		Sideband		Signal-Sideband	
	$A_{cp}^{+}(\%)$	A_{cp}^{-} (%)	A_{cp}^{+} (%)	A_{cp}^{-} (%)	A_{cp}^{+} (%)	A_{cp}^{-} (%)
0	5.6 ± 2.4	1.7 ± 2.2	4.3 ± 3.1	2.9 ± 3.5	1.3 ± 3.9	-1.2 ± 4.1
10	5.3 ± 2.4	1.7 ± 2.2	4.3 ± 3.1	2.9 ± 3.5	1.0 ± 3.9	-1.3 ± 4.1
20	5.4 ± 2.3	1.9 ± 2.2	4.8 ± 3.1	2.8 ± 3.4	0.7 ± 3.9	2.8 ± 3.4
30(nominal)	5.8 ± 2.3	2.4 ± 2.1	5.0 ± 3.0	3.4 ± 3.3	0.9 ± 3.8	-1.0 ± 3.9
40	5.1 ± 2.2	2.9 ± 2.0	4.1 ± 2.8	4.2 ± 3.1	1.0 ± 3.6	-1.3 ± 3.7

13.5 π^0 veto - cut 4

Distance (cm)	Signal		Sideband		Signal-Sideband	
	$A_{cp}^{+}(\%)$	A_{cp}^{-} (%)	A_{cp}^{+} (%)	A_{cp}^{-} (%)	A_{cp}^{+} (%)	A_{cp}^{-} (%)
No veto	5.3 ± 2.1	1.8 ± 2.0	3.2 ± 2.7	2.6 ± 3.5	2.1 ± 3.4	-0.8 ± 3.6
veto (nominal)	5.8 ± 2.3	2.4 ± 2.1	5.0 ± 3.0	3.4 ± 3.3	0.9 ± 3.8	-1.0 ± 3.9

13.6 Track Scaled Transverse Momentum (Decay Side) - Cut 1

Xpt	Signal		Sideband		Signal-Sideband	
	$A_{cp}^{+}(\%)$	A_{cp}^{-} (%)	A_{cp}^{+} (%)	A_{cp}^{-} (%)	A_{cp}^{+} (%)	A_{cp}^{-} (%)
0.020	5.7 ± 2.3	2.3 ± 2.1	4.8 ± 2.9	2.9 ± 3.2	0.9 ± 3.7	-0.7 ± 3.9
0.025(nominal)	5.8 ± 2.3	2.4 ± 2.1	5.0 ± 3.0	3.4 ± 3.3	0.9 ± 3.8	-1.0 ± 3.9
0.030	6.2 ± 2.3	2.1 ± 2.2	4.2 ± 3.0	4.1 ± 3.3	1.9 ± 3.7	2.0 ± 4.0
0.040	7.1 ± 2.4	2.2 ± 2.2	3.9 ± 3.0	4.3 ± 3.5	3.2 ± 3.9	-2.0 ± 4.0

13.7 Track $\cos\theta$ (Decay Side) - Cut 1

$\cos\theta$	Signal		Sideband		Signal-Sideband	
	$A_{cp}^{+}(\%)$	A_{cp}^{-} (%)	A_{cp}^{+} (%)	A_{cp}^{-} (%)	A_{cp}^{+} (%)	A_{cp}^{-} (%)
0.9(nominal)	5.8 ± 2.3	2.4 ± 2.1	5.0 ± 3.0	3.4 ± 3.3	0.9 ± 3.8	-1.0 ± 3.9
0.85	6.4 ± 2.3	2.0 ± 2.2	4.6 ± 3.0	4.3 ± 3.4	1.8 ± 3.8	2.3 ± 4.0
0.8	5.1 ± 3.1	1.5 ± 2.2	3.0 ± 3.1	3.3 ± 3.4	2.0 ± 3.9	3.3 ± 3.4
0.75	6.3 ± 2.6	1.5 ± 2.4	4.7 ± 3.3	4.5 ± 3.6	1.7 ± 4.1	-2.9 ± 4.3
0.7	5.3 ± 2.7	1.1 ± 2.5	6.1 ± 3.4	4.1 ± 3.8	-0.7 ± 4.3	-3.0 ± 4.5

13.8 Track scaled transverse momentum (Tag Side) - Cut 2

Xpt	Signal		Sideband		Signal-Sideband	
	$A_{cp}^{+}(\%)$	A_{cp}^{-} (%)	A_{cp}^{+} (%)	A_{cp}^{-} (%)	A_{cp}^{+} (%)	A_{cp}^{-} (%)
0.05(nominal)	5.8 ± 2.3	2.4 ± 2.1	5.0 ± 3.0	3.4 ± 3.3	0.9 ± 3.8	-1.0 ± 3.9
0.06	6.1 ± 2.3	2.9 ± 2.1	5.2 ± 3.0	3.1 ± 3.3	3.1 ± 3.3	-0.3 ± 3.9
0.07	6.0 ± 2.3	2.6 ± 2.2	5.1 ± 3.0	3.4 ± 3.3	0.9 ± 3.8	-0.8 ± 3.9
0.08	5.8 ± 2.3	2.0 ± 2.2	5.2 ± 3.0	3.6 ± 3.4	0.7 ± 3.8	-1.6 ± 4.0
0.10	5.4 ± 2.4	1.7 ± 2.2	5.5 ± 3.4	2.5 ± 3.4	-0.1 ± 3.9	-0.8 ± 4.0

13.9 Track $\cos\theta$ (Tag Side) - Cut 2

$\cos\theta$	Signal		Sideband		Signal-Sideband	
	$A_{cp}^{+}(\%)$	A_{cp}^{-} (%)	A_{cp}^{+} (%)	A_{cp}^{-} (%)	A_{cp}^{+} (%)	A_{cp}^{-} (%)
0.8(nominal)	5.8 ± 2.3	2.4 ± 2.1	5.0 ± 3.0	3.4 ± 3.3	0.9 ± 3.8	-1.0 ± 3.9
0.75	6.5 ± 2.3	2.4 ± 2.2	5.7 ± 3.0	3.3 ± 3.4	0.7 ± 3.8	-0.9 ± 4.0
0.7	5.9 ± 2.4	2.5 ± 2.3	5.9 ± 3.1	3.4 ± 3.4	-0.1 ± 3.9	0.9 ± 4.1
0.65	5.8 ± 2.5	2.5 ± 2.3	7.6 ± 3.1	2.6 ± 3.5	-1.8 ± 4.0	-0.1 ± 4.2
0.6	4.9 ± 2.6	1.5 ± 2.4	8.4 ± 3.2	2.7 ± 3.6	-3.5 ± 4.2	-1.3 ± 4.4

13.10 Track K_s Flight Distance - cut 3

Distance (mm)	Signal		Sideband		Signal-Sideband	
	$A_{cp}^{+}(\%)$	A_{cp}^{-} (%)	A_{cp}^{+} (%)	A_{cp}^{-} (%)	A_{cp}^{+} (%)	A_{cp}^{-} (%)
3.0	5.4 ± 2.2	1.7 ± 2.0	4.5 ± 2.5	2.0 ± 2.7	0.8 ± 3.3	-0.3 ± 3.4
5.0(nominal)	5.8 ± 2.3	2.4 ± 2.1	5.0 ± 3.0	3.4 ± 3.3	0.9 ± 3.7	-1.0 ± 3.9
7.0	5.7 ± 2.3	2.0 ± 2.2	4.3 ± 3.3	4.6 ± 3.7	1.4 ± 4.0	-2.5 ± 4.3

13.11 Two track separation in z for K_s - Cut 3

Distance (mm)	Signal		Sideband		Signal-Sideband	
	$A_{cp}^{+}(\%)$	A_{cp}^{-} (%)	A_{cp}^{+} (%)	A_{cp}^{-} (%)	A_{cp}^{+} (%)	A_{cp}^{-} (%)
9.0	6.4 ± 2.4	2.2 ± 2.2	4.4 ± 3.2	3.9 ± 3.6	2.0 ± 4.0	-1.6 ± 4.0
12.0(nominal)	5.8 ± 2.3	2.4 ± 2.1	5.0 ± 3.0	3.4 ± 3.3	0.9 ± 3.7	-1.0 ± 3.9
15.0	6.4 ± 2.2	2.3 ± 2.1	3.8 ± 2.8	1.6 ± 3.0	2.5 ± 3.5	0.7 ± 3.7

13.12 Two track separation in r-phi for K_s - Cut 3

Distance (mm)	Signal		Sideband		Signal-Sideband	
	$A_{cp}^{+}(\%)$	A_{cp}^{-} (%)	A_{cp}^{+} (%)	A_{cp}^{-} (%)	A_{cp}^{+} (%)	A_{cp}^{-} (%)
1.0	6.2 ± 2.3	2.8 ± 2.2	4.8 ± 3.1	2.6 ± 3.5	1.4 ± 3.9	0.2 ± 4.0
2.0(nominal)	5.8 ± 2.3	2.4 ± 2.1	5.0 ± 3.0	3.4 ± 3.3	0.9 ± 3.7	-1.0 ± 3.9
3.0	5.9 ± 2.3	2.4 ± 2.1	5.0 ± 3.0	3.2 ± 3.3	0.9 ± 3.7	-0.8 ± 3.9

14 Conclusions

A 3.5 sigma asymmetry is observed in the K-pi decay mode of the tau lepton but is attributed to either a statistical fluctation or an unknown detector effect since a control sample where we expect suppressed CP violating effects also exhibits the same asymmetry. A study of known detector effects is unable to account for such an aymmetry.

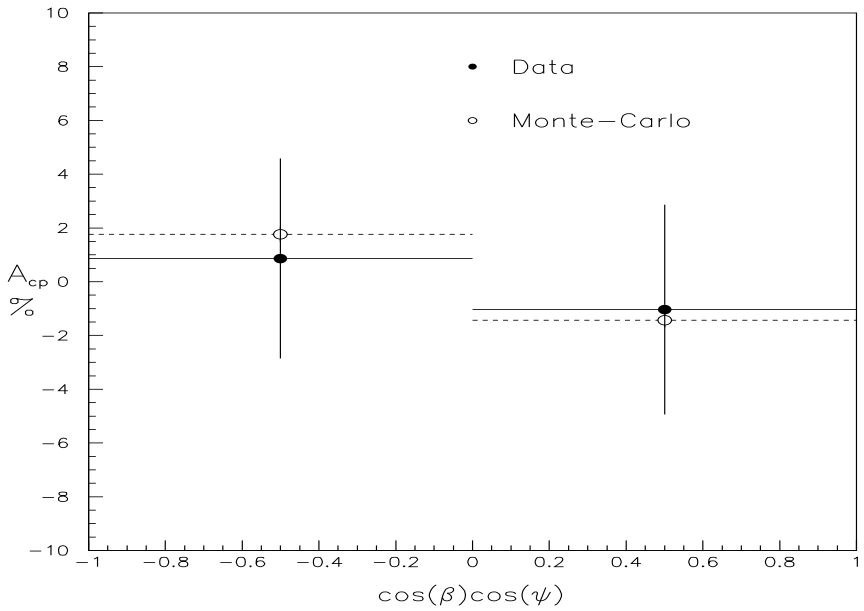

Figure 12: Measured asymmetry from data compared to monte-carlo expectation with $g = 1, \theta = \pi/2$. Errors are statistical.

Figure 12 shows both the data and the expected asymmetry for the maximal case (Im(g)=1). The expected asymmetry is diluted by a factor of 0.48 which corresponds to the purity of the $K_s\pi$ sample. We can then set limits as in appendix E on —Img— assuming mass dependent Higgs like couplings (see appendix A).

$$Im(g) = \frac{m_{tau} m_s}{m_H^2}.Im(XZ^*)$$

At 90 % C.L

$$Im(g) = \frac{m_{tau} m_s}{m_H^2}.Im(XZ^*) < 1.7$$

We have made the first search for CP violation in tau decays. This type of CP violation can occur in theories with additional scalar gauge bosons such as the Weinberg theory of CP violation. No CP violation was observed and modest limits on the imaginary part of such a Higgs coupling may be set.

15 Acknowledgement

I thank my colleagues at SLAC, Martin Perl, Helmut Marsiske, Paul Tsai and Dennis Ugolini for many helpful discussions. Help from the Caltech group (Alan Weinstein, Morris Schmitler, Jon Urheim etal) with many aspects of the analysis was greatly appreciated.

A The Three Higgs Doublet Model

In the minimal standard model there is one higgs doublet responsible for giving mass to both the gauge bosons and the fermions. The CKM matrix arises from the unitary transformations which diagonalize the quark mass matrices. An $n \times n$ unitary matrix has $n.(n-1)/2$ real independent parameters or angles and $(n-1).(n-2)/2$ independent phase angles. For three generations of quarks this implies three mixing angles and one phase. The small effects of CP violation in the kaon system are explained by the fact that the phase appears in combination with CKM elements of small magnitude. It also predicts large CP violating effects in suppressed decay modes of B mesons that have so far not been observed. No CP violating effects are expected in lepton decays.

However it is quite possible that the Higgs sector may be more complicated than just a simple doublet and many extensions to the standard model such as SUSY require a more complicated structure in order to avoid anomalies. The most likely expansion is to a set a doublets since this naturally preserves the relationship between the neutral and charged currents coupling strength. With more than one doublet we have different possibilities of which doublet couples to which quarks and leptons. If the couplings are arranged so the leptons and both up and down type quarks each couple to only one higgs doublet then flavor changing neutral currents are naturally avoided. We consider a model of 3 higgs doublets with one higgs doublet coupling to leptons one to up quarks and one to down quarks [14]. The lagrangian for the Higgs-fermion Yukawa interactions can then be written.

$$L = \overline{Q_{Li}} F^D_{ij} \phi_d D_{Rj} + \overline{Q_{Li}} F^U_{ij} \phi_u U_{Rj} + \overline{L_{Li}} F^E_{ij} \phi_e E_{Rj} +$$

where Q_{Li} denotes the left handed quark doublets and L_l the left handed lepton doublets of generation index i. The right handed quark and lepton singlets are given by D_{Rj}, U_{Rj}, E_{Rj} and the three higgs fields by ϕ_d, ϕ_u, ϕ_e. There are six charged and six neutral fields for the three higgs doublets. After symmetry breaking two charged and two neutral Goldstone bosons are eaten to give the $W^{\pm}$ and the Z masses which leaves four charged and five neutral bosons. We further consider the most general case where one of the charged bosons is much lighter in mass than the others (if there are mass degeneracies the model becomes equivalent to a two Higgs doublet model which has a different phenomenology) so that the other charged bosons effectively decouple. After diagonalizing the quark mass matrix in the usual way with unitary transformations the Lagrangian becomes

$$L = (2\sqrt{2} G_F)^{1/2} \Sigma^n_{i=2} (X_i \overline{U_L} V M_D D_R + Y_i \overline{U_R} V M_U D_L + Z_i \overline{N_L} V M_E E_R) H^{\pm}$$

X,Y,Z are complex coupling constants that give the strength of the higgs bosons to the up quarks, down quarks and leptons respectively. The charged Higgs interaction eigenstates are related to the mass eigenstates by a unitary transformation. The couplings X,Y,Z are derived from this unitary transformation.

$$\begin{pmatrix} G^{\pm} \\ H^{\pm}_2 \\ H^{\pm}_3 \end{pmatrix} = U \begin{pmatrix} \phi^{\pm}_1 \\ \phi^{\pm}_2 \\ \phi^{\pm}_3 \end{pmatrix}$$

In analogy to the CKM matrix the unitary transformation can be expressed in terms of three angles and one phase for three doublets and one angle for two doublets. It is thus possible to have a CP violating phase in the couplings with three doublets but not one or two. Since this phase can be placed on the couplings of the scalars to leptons it is thus possible to have a CP violating charged scalar interaction with the leptons. Since Higgs couplings are proportional to mass then the effects should be much more pronounced in the tau system. The Feynman rules for the interaction are shown in figure 13.

$\frac{ig}{2\sqrt{2}\,\mathrm{mW}}[(m_s X(1+\gamma_5)+m_u Y(1+\gamma_5)]V_{us}$ $\qquad$ $\frac{ig}{2\sqrt{2}M_W} m_l Z(1+\gamma_5)$

Figure 13: Feynman rules for couplings in three Higgs doublet model

For the decay $\tau \to K_s h\nu$ the relevant CP violating coupling combination is

$$Im(XZ^*)$$

These models are disfavoured as a complete theory of CP violation [13] since the constraints from the limits on the neutron electric dipole are difficult to reconcile with the observed CP violation in the kaon system. It is however quite possible that it may be a partial explanation of CP violation.

B Baryogenesis

There is strong evidence that the universe is made of matter rather than anti-matter. This is usually quantified in terms of the Baryon number per unit comoving volume which is a constant in the absence of Baryon number violating interactions.

$$n_B = \frac{n_b - n_{\overline{b}}}{s}$$

$n_{b(\overline{b})}$ is the baryon(antibaryon) number density and s is the entropy density which is related to the photon density. The planets and Sun are made of matter. Cosmic rays contain only a small fraction of antiprotons (10^{-4} compared to protons) which is consistent with being produced by the collision of protons with the interstellar medium. This implies that the galaxy is made of matter. This leaves the possibility of large extragalactic structures of antimatter which would give an overall baryon symmetric universe. However if we start with a baryon symmetric early universe then baryons and anti baryons remain in equilibrium down to a temperature of 22 MeV when $n_B = 7 \times 10^{-20}$ which is 9 orders of magnitude greater than the current value of $3.81 \times 10^{-9} \Omega h^2$. This implies then that large chunks of antimatter would have to be separated out at an early time which was causally impossible. The most reasonable conclusion is that at early times the universe possessed a significant asymmetry between the number of baryons and antibaryons which prevented them from coming into equilibrium. Although the baryon asymmetry is maximal today at early times the asymmetry would have been much smaller

$$n_B = \frac{n_q - n_{\overline{q}}}{n_q} \simeq 10^{-8}$$

Baryogenesis provides a model of how an initially baryon symmetric universe evolves dynamically into completely baryon asymmetric universe.

To generate an asymmetry from an Initially symmetric universe three conditions are required.

- Baryon Number Violation. This requires interactions that convert quarks into leptons or antiquarks. Such interactions occur in GUT models with large mass bosons propagating the interactions so that they are so weak at current energy scales as to be unobservable.

- C and CP violation. C and P violation is maximal in weak interactions and CP violation has been observed in the Kaon system.
- Out of Thermal equilibrium conditions. Essentially this is provided by the expansion of the universe.

  If the CP violation is provided solely by the CKM standard model of CP violation and baryogenesis is correct then the baryon number asymmetry is eight orders of magnitude less than currently observed [36]

C CP violating Detector effects

There are a variety of known effects that may cause inefficiencies between positive and negative particles in particle detectors. We discuss some of the possibilities at CLEO

C.1 Tracking Effects

AT CLEO It is known that the tracking efficiency is very slightly different for low energy (< 250 MeV) π^+ and π^- [35]. Misalignments between the different tracking detectors can cause a different measured curvature between for positive and negative tracks [21]. In addition other geometric effects may arise due to the different lorentz angle for drifting electrons from positive and negative tracks which means the electrons pass through different parts of a drift cell which is slightly non-uniform. Figure 14 shows the tracking asymmetry (A^π) for low energy pions. We use a sample of 2 million $K^0_s \to \pi^+\pi^-$ from 4s2-4sG where the track and the KS are identical to our signal definition. The momentum distribution for pions from $K^0_s \to \pi^+\pi^-$ decays is used since the distribution for π^+ and π^- should be identical in the absence of inefficiencies. It can be seen that π^+ are reconstructed slightly more efficiently than π^- for low momentum.

$$A^\pi = \frac{N(p)^+ - N(p)^-}{N(p)^+ + N(p)^-}$$

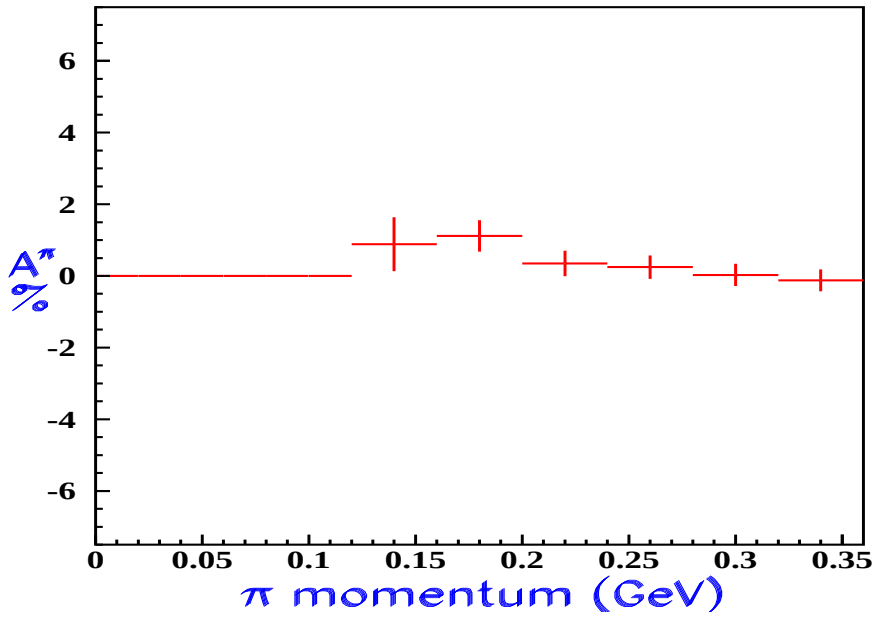

Figure 14: Asymmetry versus momentum due to tracking inefficiencies for low energy pions.

C.2 Calorimetric Effects

There are also calorimetric effects. The nuclear interaction of charged hadrons with Cesium iodide is substantially different for positive and negative [24] tracks. Figure 15 shows the different crossections for π^+ and π^- interactions with protons. The crossections are dominated by resonances below a momentum of 1 GeV.

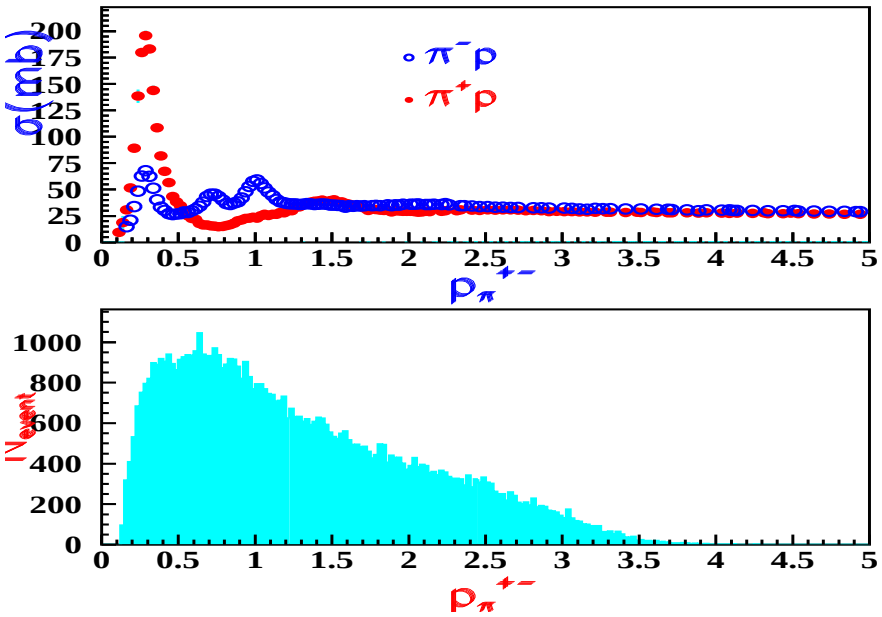

Figure 15: Total Cross-sections for $\pi^{\pm}$ with protons taken from the PDG [24]. Also shown is the momentum distribution for charged pions from the decay $\tau^{\pm} \to K_s^0 \pi^{\pm} \nu_\tau \qquad K_s^0 \to \pi^+ \pi^-$

In particular these nuclear interactions can produce electromagnetic deposits in the calorimeter which can be substantially displaced from the track intersection point (hadronic split-offs). Figure 16 shows the asymmetry in the number of clusters $N(d)^{\pm}$ at a distance d from the projection of a π^+ and π^- track.

$$A_{cluster} = \frac{N(d)^+ - N(d)^-}{N(d)^+ + N(d)^-}$$

We use the pions from the $K_S^0 \to \pi^+\pi^-$ sample described in the previous section.

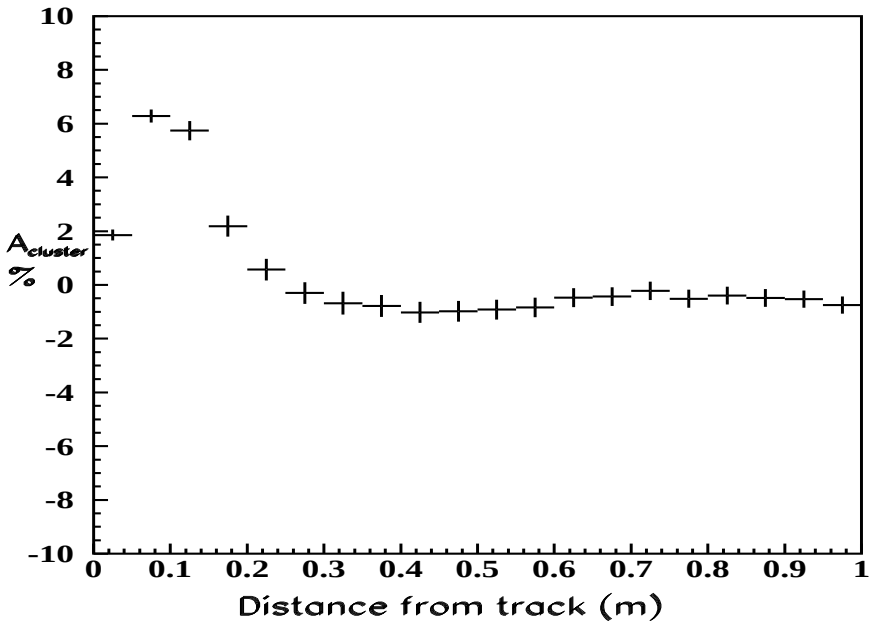

Figure 16: $A_{cluster}$ for all clusters versus disstance from π^+ and π^- track projections

It can be seen that there are significantly more clusters about a π^+ cluster than about a π^- cluster. We have two veto's on electromagnetic clusters. First we veto on clusters identified as good photons with energy greater than 100 MeV, not matched to a track and not within 30 cm of a track. Figure 17 shows the asymmetry for the number of such photons $N(d)^{\pm}$ at a distance d from the track.

$$A_{veto_photons} = \frac{N(d)^+ - N(d)^-}{N(d)^+ + N(d)^-}$$

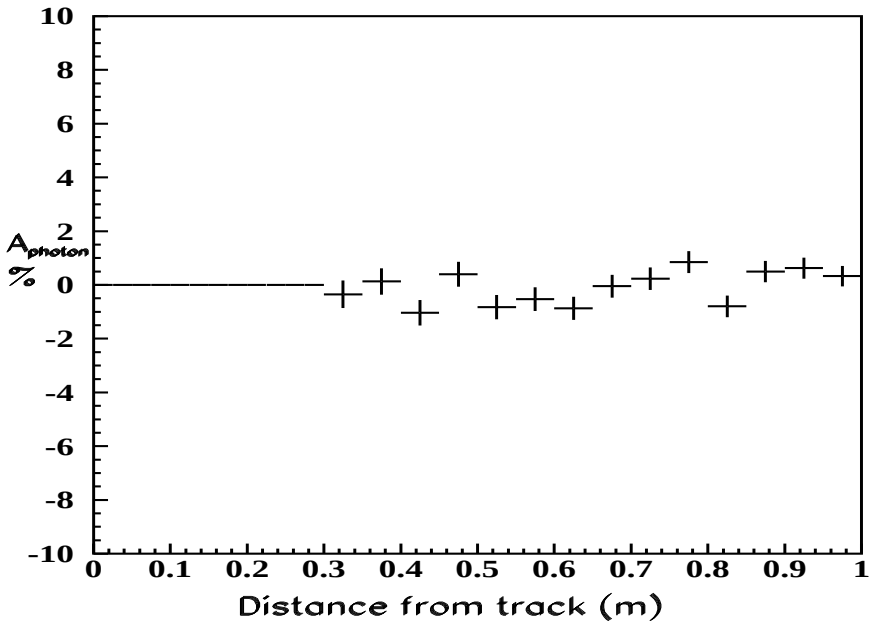

Figure 17: $A_{veto_photons}$ for veto photons versus disstance from π^+ and π^- track projections

It can be seen that the asymmetry is zero so that vetoing on these photons should provide no spurious asymmetry. Secondly we veto on unmatched clusters with energy greater than 350 MeV on the signal side of the event to remove K_L^0 backgrounds. Figure 18 shows the asymmtery for these clusters.

$$A_{veto_clusters} = \frac{N(d)^+ - N(d)^-}{N(d)^+ + N(d)^-}$$

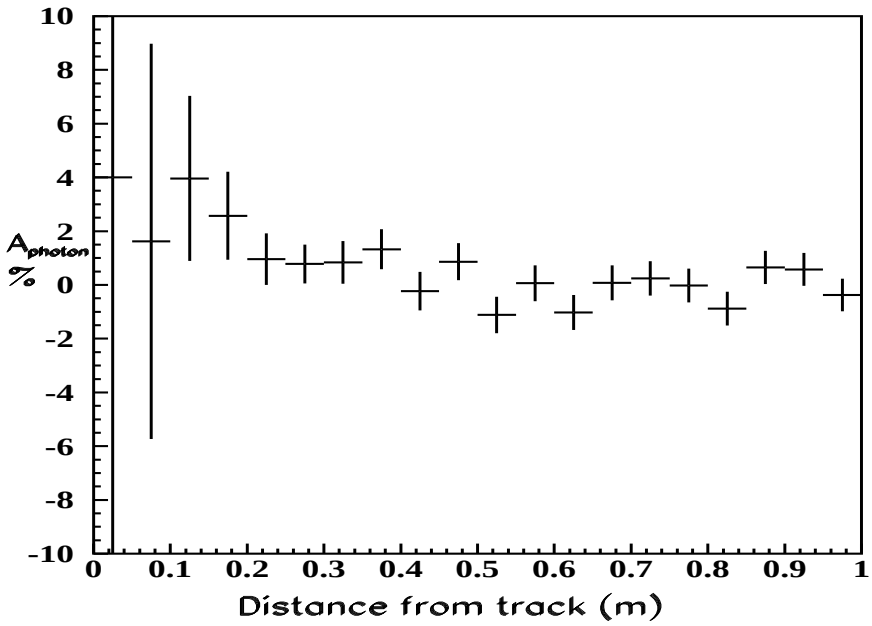

The

Figure 18: $A_{veto_clusters}$ for veto clsuters versus distance from π^+ and π^- track projections

asymmetry is non-zero so that vetoing on these clusters can provide a fake asymmetry. The unmatched photon/cluster veto cut used in most tau analysis is an extremely powerful cut for rejecting background and can not be avoided if one hopes to obtain a relatively clean sample. Unfortunately these hadronic split-offs are known to be very poorly modeled in the CLEO monte-carlo.

C.3 K_S^0 reconstruction

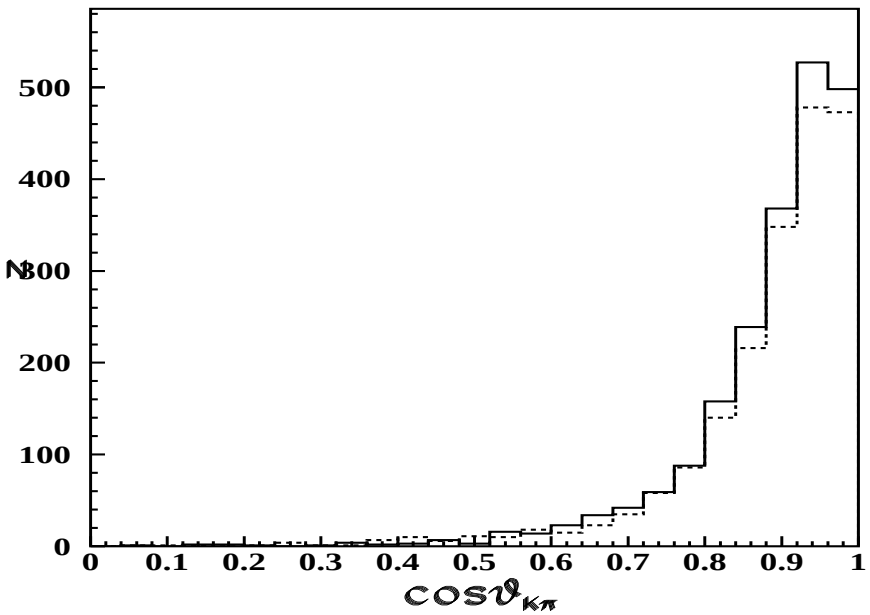

Figure 19: The cosine of the angle between K_S^0 and π for $K_S^0\pi^+$ and $K_S^0\pi^-$ from the dataset

Figure 19 shows the cosine of the angle between the K_S^0 direction and the π^+/π^- for the $K_S^0\pi$ signal sample. It can be see that pion is produced in close proximity to the K_S^0 and further that it is more likely to be in proximity to a π^+ than a π^+. To investigate whether there is some systematic difference in reconstruction efficiency of the K_S^0 in close proximity to a π^+ as opposed to a π^- we use the large sample of $K_S^0 \to \pi^+\pi^-$ described in the previous section and plot the angle between the pion and the K_S^0 for π^+ and π^-. We then derive an asymmetry from these distributions as in figure 20. It can be seen that there is a small asymmetry which could fake CP violation.

$$A_{cos} = \frac{N(cos)^+ - N(cos)^-}{N(cos)^+ + N(cos)^-}$$

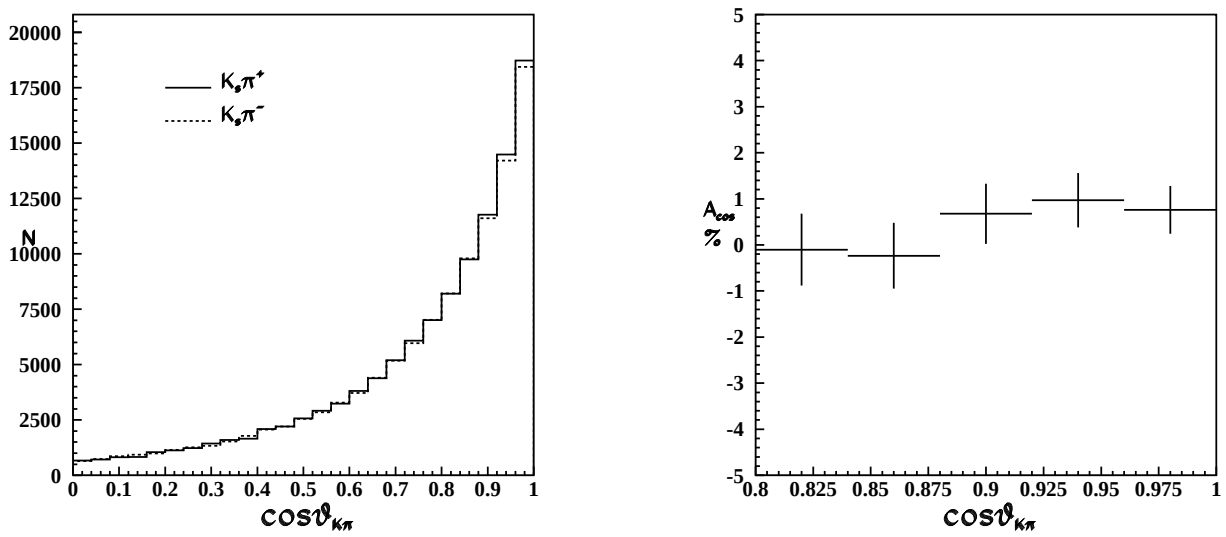

Figure 20: The distributions of $K^0_S\pi^+$ and $K^0_S\pi^-$ and the derived asymmetry A_{cos}.

D CP Violation in $\tau^- \to \pi^-\pi^+\pi^-\nu$

The possibility of CP violation in the three pion decay mode of the tau lepton has been considered by several authors [37], [38]. In section 10 we argued that the observable CP violation in the three pion mode should be suppressed relative to the K-pi mode and hence that we can use the sidebands of figure 9 as a control sample. We can test this supposition experimentally by defining an independent $\tau^- \to \pi^-\pi^+\pi^-\nu$ sample of high purity and looking for an asymmetry in the same way as for the k-pi analysis. We define a high purity sample using only the the lepton tags as in a previous published CLEO analysis [39]. We use identical cuts on the full CLEO II tau data set (4.41×10^6 tau pairs) to yield a total of 44664 events in agrrement with MC expectations of 44362 ± 1413 events.
The three pi mass is shown in figure 21 for comparison with figure 2of reference [39].

	N Events Data	N Events Expected
e-3h	28041	27461 ± 1204
mu-3h	17523	16901 ± 740
Total	44664	44362 ± 1413

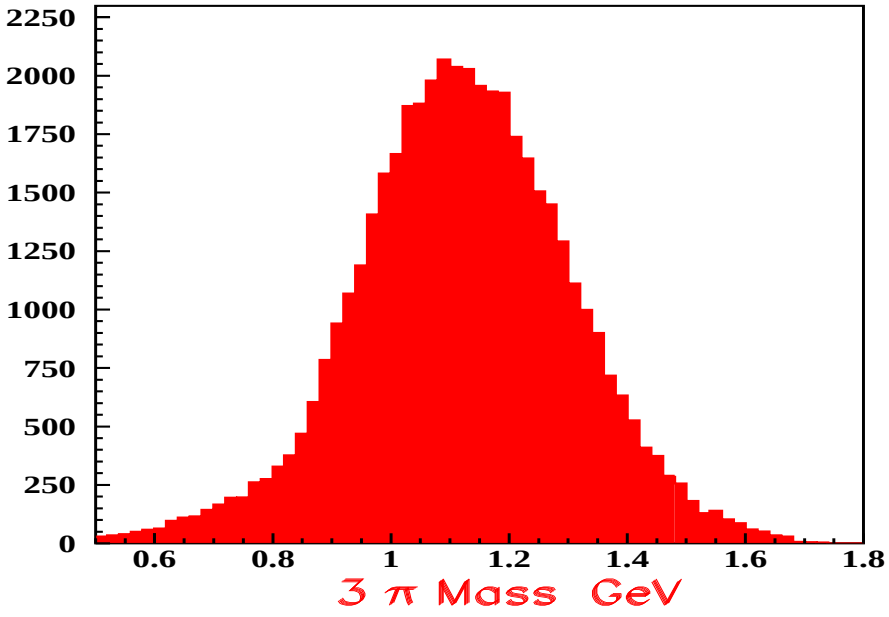

Figure 21: 3 pion invariant mass of $\tau^- \to \pi^-\pi^+\pi^-\nu$ candidates

The cuts used to define the $\tau^- \to \pi^-\pi^+\pi^-\nu$ dataset differ from the K-pi analysis as follows:

Cut Description	3pi	K-pi
tag mode	electron $(P/E_{beam} > 0.10, \lvert cos\theta\rvert < 0.71)$ muon $(P/E_{beam} > 0.26, \lvert cos\theta\rvert < 0.71)$	1 track $(P/E_{beam} > 0.05, \lvert cos\theta\rvert < 0.71)$ $+ \leq 1\pi^0$
signal hadrons	3 tracks $(P/E_{beam} > 0.05, \lvert cos\theta\rvert < 0.80)$	3 tracks $(P/E_{beam} > 0.025, \lvert cos\theta\rvert < 0.90)$
3track invariant mass	3 pi mass < 1.777	No requirement
K_s^0	Veto events with K_s^0	Require K_s^0
Photon veto	$E > 100$ MeV signal and tag side	$E > 300$ MeV tag $E > 100$ Mev signal
Cluster veto	$E > 800$ MeV signal and tag sides	$E > 350$ MeV signal side
E_{vis}	No Requirement	$0.7 < E_{vis} < 1.7$
Missing Momentum	$\lvert\cos\theta\rvert$ of $\vec{P^{miss}} < 0.9$	$\vec{P^{miss}} > 0.03, \lvert\cos\theta\rvert < 0.95$

The two datasets are independent by virtue of the K_s^0 requirements. The threshold cuts (track momenta and photon veto) are tighter for the 3pi analysis and there is no 3 pi mass cut in the k-pi analysis. Using the 3pi dataset we measure the asymmetry as

	N Events	$A_{cp}^+(\%)$	$A_{cp}^+(\%)$
e-3h	28041	0.27 ± 0.60	0.17 ± 0.61
mu-3h	17523	-0.46 ± 1.1	-0.33 ± 1.1
Total	44664	-0.013 ± 0.47	-0.023 ± 0.47

There is no evidence for an any statistically significant asymmetry. To check

that the slight difference in the cuts has no effect we use the a1 thershold cuts on the $K^0_S\pi$ sample

	N Events	$A^+_{cp}(\%)$	$A^+_{cp}(\%)$
$K^0_S\pi$	1193	8.7 ± 4.2	1.9 ± 4.0

The asymmetry still remains. Further we use the K-pi threshold cuts on a sample of events from the tau skims. Here we explicitly exclude events with a K^0_S candidate within 30 MeV of the K^0_S mass. There is no evidence for any asymmetry in this sample.

	N Events	$A^+_{cp}(\%)$	$A^+_{cp}(\%)$
Tau skim	37512	-0.56 ± 0.74	0.78 ± 0.76

E Setting Limits

Let the measured values of the asymmetry be $(A^-_m \pm \sigma_m, A^+_{m+} \pm \sigma_m)$ and the expected values of the asymmetry (A^-_e, A^+_{e+}) where $\sigma_e \ll \sigma_m$ and the errors are Gaussian. The probability of this measurement is then

$$P_m = (1 - Erf(\frac{A^-_m - A^-_e}{\sigma_m}).(1 - Erf(\frac{A^+_m - A^+_e}{\sigma_m}))$$

where

$$Erf(x) = \int_{-\infty}^{x} exp^{-t^2/2} dt$$

To exclude (A^-_e, A^+_e) at 90 % confidence limit we require

$$P_m < (1.0 - 0.9) = 0.1$$

Using the expected values $(A^-_e = -1.6Im(g)\%, A^+_{e+} = 1.6Im(g)\%)$ and the measured values $(A^-_m = 0.9 \pm 3.8\%, A^+_{m+} = -1.0 \pm 3.9\%)$ we tabulate the probability of obtaining the measured values for different values of Im(g). We can then exclude $|Im(g)| > 1.7$ at 90 % C.L

Im(g)	P_m
-3.0	0.03
-2.0	0.08
-1.7	0.10
-1.0	0.19
1.0	0.06
2.0	0.02
3.0	0.005

References

[1] R. Mohapatra and P. Pal "Massive Neutrinos and Astrophysics" Chapter 12.2, World Scientific.

[2] S. Glashow,A.G. Cohen, A. De Rujula "A MATTER - ANTIMATTER UNIVERSE?" BUHEP-97-19, Jul 1997.

[3] "BARYONIC ASYMMETRY OF THE UNIVERSE" By A.D. Sakharov (Lebedev Inst.) Sov.Phys.JETP 49:594-599,1979

[4] "ELECTROWEAK BARYOGENESIS AND STANDARD MODEL CP VIOLATION." P Huet, E Sather Phys. Rev. D **51**, 379 (1995)

[5] G. Luders "Proof of the TCP theorem" Ann. Phys. 2, 1(1957)

[6] I. Dunietz and J. Rosner "Time dependent CP violation effects in $B_0 - \overline{B^0}$ systems" Phys. Rev. D **34**, 1404 (1986)

[7] M. Bander, D. Silverman and A. Soni "CP non-invariance in the Decays of Heavy Charged Quark Systems" Phys. Rev. Lett. **43**, 242 (1979)

[8] S. Barr and W. Marciano "Electric Dipole Moments" in "CP Violation" p. 455 edited by C. Jarlskog - World Scientific 1988

[9] J. Donoghue, X. He and S. Pakvasa "Hyperon decays and CP nonconservation" Phys. Rev. Lett. **34**, 833 (1986)

[10] J. Donoghue, B. Holstein and G. Valencia "Survey of Present and Future tests of CP violation" Int. Journal Mod. Phys. 2 319 1987

[11] T.D. Lee Phys. Rev. D **8**, 1226 (1973)

[12] S. Weinberg "Gauge Theory of CP violation" Phys. Rev. Lett. **37**, 657 (1976)

[13] S. Krawczyk and S Pokorski "Constraints on CP violation by a non-minimal Higgs sector from CP conserving processes" Nucl. Phys. B **364**, 10 (1991)

[14] Y. Grossman "Phenomenology of models with more than two Higgs doublets" Nucl. Phys. B **426**, 355 (1994)

[15] W. Bernreuther *et al.*"CP violating effects in Z decays to τ leptons" Z. Phys. C **52**, 567 (1991)

[16] R. Akers *et al.*OPAL collaboration "A test of CP-invariance in $Z^o \to \tau^+\tau^-$ using optimal observables" Z. Phys. C **66**, 31 (1995)

[17] J. Kuhn "Tau Kinematics from Impact Parameters" Phys. Lett. B **313**, 458 (1993)

[18] CLEO collaboration "Determination of the Michel Parameters and the τ Neutrino Helicity in τ Decay" Phys. Rev. D **56**, 5320 (1997)

[19] Y.S Tsai "Decay correlations of heavy leptons in $e^+e^- \to l^+l^-$" Phys. Rev. D **4**, 2821 (1971)

[20] M. Davier *et al.*"The Optimal method for the Measurement of Tau Polarization" Phys. Lett. B **306**, 411 (1993)

[21] N. Wermes "CP Tests and Dipole Moments in τ-Pair Production experiments" Talk at Tau 96, Aspen Colorado 1996

[22] W. Bernreuther O. Nachtman "CP Violating Correlations in Electron-Positron Annihilation into τ leptons" Phys. Rev. Lett. **63**, 2787 (1989)

[23] D. Perkins "Introduction to High Energy Physics" P. 125

[24] Particle Data Group "Review of Particle Physics 1996" Phys. Rev. D **54**, 1 (1996)

[25] Y.S. Tsai "Production of polarized τ pairs and tests of CP violation using polarized $e^{\pm}$ colliders near threshold" Phys. Rev. D **51**, 3172 (1995)

[26] Y.S. Tsai "Search for New Mechanism of CP violation through τ decay and Semileptonic decay of hadrons" Talk at Tau 96, Aspen Colorado 1996

[27] J. Kuhn and F. Wagner "Semileptonic Decays of the tau lepton" Nucl. Phys. B **236**, 16 (1984)

[28] J. Kuhn and E. Mirkes "CP Violation in semileptonic τ decays with unpolarized beams" Phys. Lett. B **398**, 407 (1997)

[29] S. Jadach, J. Kuhn and Z. Was "TAUOLA - a library of monte carlo programs to simulate decays of polarized τ leptons" Computer Physics Communications 64 1991 275

[30] A. Weinstein and M. Schmidtler. Private Communication

[31] S. Roberts "Trkman the next generation - The quest for track quality" CLEO internal note - CBX 96-103

[32] B Heltsley "SEID/SMID A simple electron/muon id package for tau physics" CLEO internal note - CBX 93-108

[33] The π^0 are reconstructed from pairs of calorimeter showers which are not matched to tracks ($E_\gamma > 50MeV, \mid \cos\theta \mid < 0.70$ $E_\gamma > 30MeV, 0.70 \mid \cos\theta \mid < 0.95$. The invariant mass is required to be within 5 σ of the true π^0 mass.

[34] S. Chan "A Measurement of the Branching fractions for $\tau \to K^0_s h^- \nu_\tau$" CLEO internal note - CBX 96-85

[35] K. Cho CLEO internal note - CBX 93-77

[36] S. Barr,Gino Segre and H Weldon, Phys. Rev. D **20**, 2494 (1979)

[37] S.Y. Choi, K. Hagiwara and M. Tanabashi Phys. Rev. D **52**, 1614 (1995)

[38] Y.S. Tsai SLAC-PUB 7728 1998

[39] "Measurements of the Decays $\tau^- \to \pi^-\pi^+\pi^-\nu$ and $\tau^- \to \pi^-\pi^+\pi^-\pi^0\nu$ R. Balest *et al.*CLEO Collaboration Phys. Rev. Lett. **75**, 3809 (1995)